**Statistical Analysis.** Statistical analysis was performed by using Student's $t$ test and the $\chi^2$ test. $P < 5\%$ was considered to have a statistical significance.

## Results

**Establishment of Intra-MHC Recombinant-Congenic New Zealand Mice.** By selective backcrossing, we first introduced the H-$2^{g2}$ haplotype derived from the B10.GD strain into NZB (H-$2^d$) and NZW (H-$2^z$) and established H-2-congenic NZB.GD (20) and NZW.GD strains. H-$2^{g2}$ has an intragenic recombination between d and b haplotype in the $E$ gene and the H-2 haplotype is $K^dAb^dAa^dEb^dEa^bTnfa^bD^b$ (Table 1) (32). Because the $Ea^b$ gene is defective, H-$2^{g2}$ mice do not express E molecules (20). To establish the strain that carries the H-2 haplotype of $K^dAb^dAa^dEb^dEa^dTnfa^bD^b$, we conducted a search for the mouse with a spontaneously occurring intragenic recombination between $Ea$ and $Tnfa$ in the progeny of NZB and NZB.GD crosses. In ≈3,000 meiosis, there was a single mouse carrying this recombination, and the recombination-congenic NZB line, provisionally designated NZB.GDr (H-$2^{g2r}$), was generated. This haplotype is valid to evaluate the effect of E molecule expression on the same $Tnfa^bD^b$ background. Table 1 summarizes the haplotypes of the intra-MHC-congenic New Zealand mouse and the related strains.

**E Molecule Expression Levels in (NZB × NZW)$F_1$ Mice with Different Intra-H-2 Haplotypes.** Congenic and recombinant-congenic New Zealand mice were crossed to obtain (NZB × NZW)$F_1$ mice with four different combinations of the H-2 haplotype (Table 1). Fig. 1 shows flow cytometric analyses for expression profiles of A, E, and D molecules on peripheral blood lymphocytes. As expected, although levels of $A^d$ expression were almost identical, levels of E molecules differed significantly among these $F_1$ mice, i.e., full expression levels in H-$2^{d/d}$ homozygous, approximately one-half of expression levels in H-$2^{d/g2}$ and H-$2^{g2r/g2}$ heterozygous, and no expression in H-$2^{g2/g2}$ homozygous $F_1$ mice. Profiles of the class I D molecule expression showed that lymphocytes from H-$2^{d/g2}$ $F_1$ mice were positive for both $D^d$ and $D^b$, whereas those from H-$2^{g2r/g2}$ and H-$2^{g2/g2}$ $F_1$ mice were positive for $D^b$ and negative for $D^d$. As also shown in Fig. 1, E molecules in wild-type H-$2^{d/z}$ heterozygous $F_1$ mice were fully expressed. Because these $F_1$ mice are heterozygous H-$2^{d/z}$, the level of $A^d$ and $D^d$ expression was approximately one-half of that seen in the H-$2^{d/d}$ homozygote.

**Comparisons of Disease Features.** Fig. 2*A* compares cumulative incidences of proteinuria in wild-type H-$2^{d/z}$ heterozygous (NZB × NZW)$F_1$ mice with intact E molecule expression and four kinds of H-2-congenic (NZB × NZW)$F_1$ (H-$2^{d/d}$, H-$2^{d/g2}$, H-$2^{g2r/g2}$, and H-$2^{g2/g2}$) carrying identical homozygous $A^{d/d}$ molecules but different levels of E molecule expression. Compared with findings in wild-type $F_1$ mice, the incidence was markedly reduced in homozygous $A^{d/d}$ $F_1$ mice with intact E molecule expression (H-$2^{d/d}$). In a striking contrast, homozygous $A^{d/d}$ $F_1$ mice deficient in E expression (H-$2^{g2/g2}$) showed an early onset and a high incidence of proteinuria comparable to those found in the wild-type $F_1$ mice. Findings in H-$2^{d/g2}$ and H-$2^{g2r/g2}$ with one-half of E expression levels were in between. Together with the finding that heterozygous H-$2^{g2r/g2}$ and homozygous H-$2^{g2/g2}$ $F_1$ mice share the same H-2 haplotype except for the $Ea$ subregion (Table 1), it is strongly suggested that the development of lupus nephritis in $A^{d/d}$ $F_1$ mice is down-regulated by E molecules in a dose-dependent manner.

As shown in Fig. 2*B*, the decrease in survival rate was associated with an increase in the incidence of proteinuria in all groups of mice. Whereas all H-$2^{g2/g2}$ $F_1$ mice and 90% of wild-type $F_1$ mice died of disease by 12 months of age, 80% of H-$2^{d/d}$ $F_1$ mice and ≈50% of H-$2^{d/g2}$ and H-$2^{g2r/g2}$ $F_1$ mice remained alive. In Fig. 2 *C* and *D*, we compare serum levels of IgG autoantibodies to DNA and to chromatin, respectively, in 6-month-old homozygous $A^{d/d}$ $F_1$ mice with different levels of E expression. Whereas H-$2^{g2/g2}$ $F_1$ mice lacking E molecules showed high levels of both autoantibodies, comparable to those found in wild-type $F_1$ mice, the levels were greatly reduced in mice expressing E molecules.

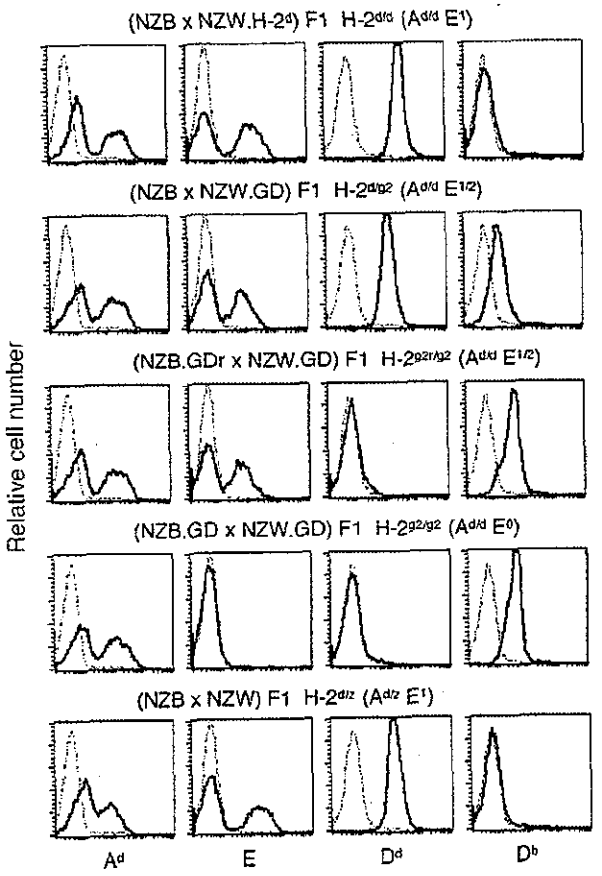


Fig. 1. Flow cytometry analysis for cell surface expression of $A^d$, E, $D^d$, and $D^b$ molecules on peripheral lymphocytes in (NZB × NZW)$F_1$ mice with different H-2 haplotypes. The upper four groups of $F_1$ mice with homozygous $A^{d/d}$ showed the same expression level of $A^d$ molecules, and the level in wild-type H-$2^{d/z}$ heterozygous $F_1$ mice was almost one-half of that seen in the former groups. When E molecule expression levels were examined with a mAb to a common determinant, H-$2^{d/g2}$ and H-$2^{g2r/g2}$ $F_1$ mice showed approximately one-half the level ($E^{1/2}$) of that seen in H-$2^{d/d}$ and wild-type H-$2^{d/z}$ $F_1$ mice ($E^1$). H-$2^{g2/g2}$ $F_1$ mice did not express E molecules ($E^0$). $D^d$ expression levels in H-$2^{d/g2}$ and H-$2^{d/z}$ $F_1$ mice were approximately one-half of that seen in H-$2^{d/d}$ $F_1$ mice. $D^b$ expression level in H-$2^{d/g2}$ $F_1$ mice was approximately one-half of that seen in H-$2^{g2r/g2}$ and H-$2^{g2/g2}$ $F_1$ mice.

**Increase in Activated T Cells in E-Deficient Mice.** Frequencies of $CD69^+$ activated $CD4^+$ T cells increase with age in (NZB × NZW)$F_1$ mice, as animals develop SLE (33). Fig. 3*A* compares frequencies of $CD69^+$ activated splenic $CD4^+$ T cells in total $CD4^+$ T cells among four groups of $A^{d/d}$ $F_1$ mice at 6 months of age. The frequency (mean ± SE) in E-negative H-$2^{g2/g2}$ $F_1$ mice (31.1 ± 8.6) was significantly higher than those found in three other groups of $F_1$ mice (11.0 ± 2.2 in H-$2^{d/d}$ $F_1$ mice, 14.2 ± 4.6 in H-$2^{d/g2}$ $F_1$ mice, and 17.2 ± 6.3 in H-$2^{g2r/g2}$ $F_1$ mice) ($P < 0.02$). Frequencies in H-$2^{d/g2}$ and H-$2^{g2r/g2}$ $F_1$ mice showed a tendency to be higher than those found in H-$2^{d/d}$ $F_1$ mice; however, there were no significant differences among the groups.

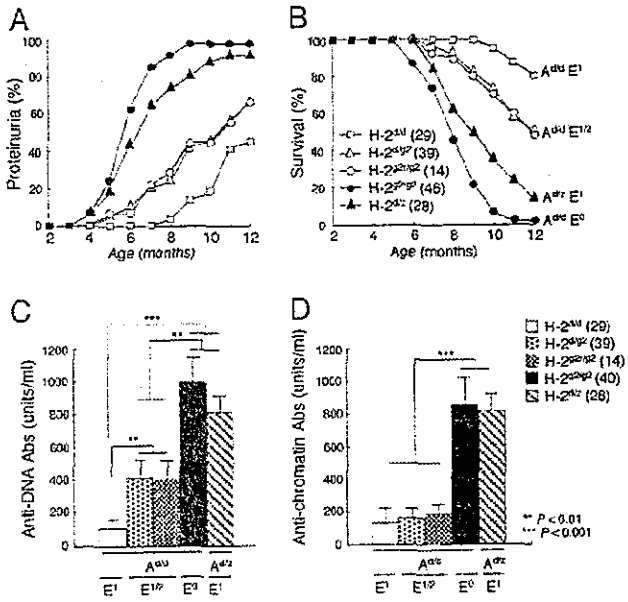


Fig. 2. Comparisons of the cumulative incidence of proteinuria (*A*), survival rate (*B*), and serum levels of IgG anti-DNA antibodies (*C*) and anti-chromatin antibodies (*D*) among $F_1$ mice with different H-2 haplotypes. The number of mice examined is shown in parentheses. H-$2^{g2/g2}$ $F_1$ showed a significantly higher incidence of proteinuria and a lower survival rate, as compared with three other $A^{d/d}$ $F_1$ strains ($P < 0.001$). Incidence of proteinuria and survival rate in H-$2^{d/d}$ $F_1$ mice were significantly reduced, as compared with H-$2^{d/g2}$ $F_1$ and H-$2^{g2r/g2}$ $F_1$ mice ($P < 0.01$). Compared with H-$2^{g2/g2}$ $F_1$ mice, wild-type H-$2^{d/z}$ $F_1$ mice showed a subtle but significantly lower incidence of proteinuria after 7 months of age ($P < 0.05$) and an improved survival rate after 9 months of age ($P < 0.05$). Serum levels of autoantibodies are compared at 6 months of age. Column and bar represent mean and SE, respectively. Asterisks indicate a significant difference.

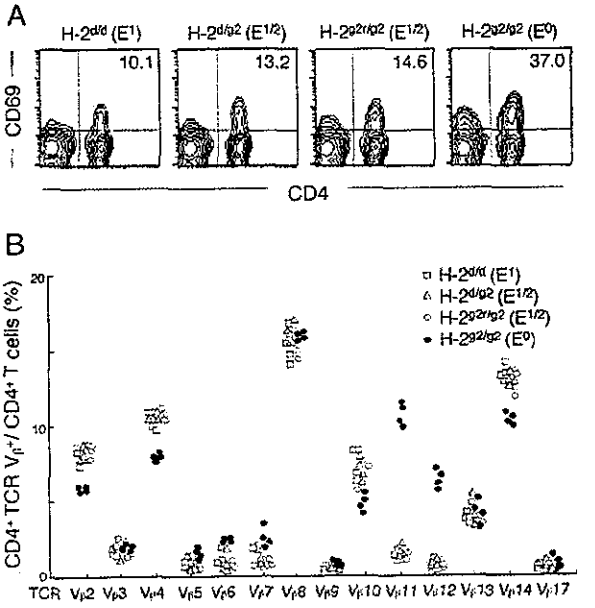


Fig. 3. Changes in splenic $CD4^+$ T cells among 6-month-old $A^{d/d}$ $F_1$ mice with different E molecule expression levels. (*A*) Representative flow cytometry profiles for the expression of activation marker CD69 on splenic $CD4^+$ T cells. Frequency of $CD69^+CD4^+$ T cells per total $CD4^+$ T cells is shown. (*B*) Comparisons of each TCR $V_\beta$ repertoire frequency in splenic $CD4^+$ T cells. $V_\beta 11$ and $V_\beta 12$ repertoires were significantly higher in H-$2^{g2/g2}$ $F_1$ mice than those in other three $F_1$ mice ($P < 0.001$).

**TCR $V_\beta$ Repertoire Skewing in E-Deficient Mice.** E molecule expression levels on thymic epithelial cells affect TCR $V_\beta$ repertoire selection in the thymus (34–36). As shown in Fig. 3*B*, $V_\beta 11$ and $V_\beta 12$ repertoires in splenic $CD4^+$ T cells were negatively selected in E molecule-positive H-$2^{d/d}$, H-$2^{d/g2}$, and H-$2^{g2r/g2}$ $F_1$ mice, and there was no significant difference in these repertoire frequencies among the three groups. In contrast, significant proportions of $V_\beta 11$ (mean and SE, 10.8 ± 0.2%) and $V_\beta 12$ (6.0 ± 0.3%) repertoires were observed in E-negative H-$2^{g2/g2}$ $F_1$ mice.

**Effects of E Molecule Expression on DC Function.** Differences in haplotypes of class II molecules may affect autoimmune manifestations through the self-antigen presenting capacity of antigen-presenting cells. To determine whether the presence or absence of E molecules affects the potential for self-antigen presentation, we took advantage of a T cell proliferation assay against self-antigen. Splenic T cells from (NZB × NZW)$F_1$ mice were transfected *in vitro* with chromatin-specific TCR $V_\alpha$ and $V_\beta$, originally derived from a (SWR × NZB)$F_1$ mouse, which can recognize the immunodominant nucleosomal epitope (amino acids 71–94 in histone H4) in the context of $A^{d/d}$ (27, 28) and other A haplotype molecules (37). These T cells can reconstitute the specificity to the nucleosome (38). Such T cells and the T cells transfected with vector alone (mock) were cocultured with CD11c-positive splenic DCs obtained from (NZB × NZW)$F_1$ with different levels of E expression, in the presence of chromatin. As shown in Fig. 4, although DCs from $A^{d/d}$ $F_1$ mice with H-$2^{d/d}$, H-$2^{d/g2}$, and H-$2^{g2/g2}$ haplotypes induced significant levels of chromatin-specific T cell responses, there were no significant differences among the three groups of $F_1$ mice. Compared with findings in these $A^{d/d}$ $F_1$ mice, DCs from wild-type $A^{d/z}$ heterozygous (NZB × NZW)$F_1$ mice induced a significantly greater response of chromatin-specific T cells. Thus, it is suggested that, as compared with $A\alpha^d\beta^d$, $A^{d/z}$-unique $A\alpha^d\beta^z$ and/or $A\alpha^z\beta^d$ have an increased capacity of DCs to present chromatin and that the presence or absence of E molecules does not influence the potential of DCs for chromatin presentation.

## Discussion

Our newly generated intra-MHC recombinant-congenic (NZB × NZW)$F_1$ mice make it feasible to examine the role of class II A and E molecules in the regulation of autoimmune disease, with disregard to the effect of other MHC genes such as *Tnfa* and class I D, which also have been implicated in autoimmune susceptibility (39, 40). The results clearly indicated that class II A and E serve as promoting and protective genetic elements, respectively.

H-$2^{d/z}$ heterozygosity has a strong impact on SLE in (NZB × NZW)$F_1$ mice, because the disease is largely reduced in H-$2^{d/d}$ and H-$2^{z/z}$ homozygous mice (2, 3, 5). This observation means that a combination of H-2-linked genes from both parents play a role in an epistatic manner. In this context, we earlier speculated that the polymorphic class II $\alpha$ and $\beta$ chain genes from both parents may form $F_1$-unique mixed haplotype $\alpha/\beta$ heterodimers, such as $A\alpha^d\beta^z$ and $A\alpha^z\beta^d$, either of which may serve as a restriction element for self-reactive T cells (5). Consistent was the finding in the present studies that, compared with DCs from $A^{d/d}$ homozygous $F_1$ mice, DCs from wild-type $A^{d/z}$ (NZB × NZW)$F_1$ mice showed a greater likelihood of chromatin presentation to T cells. Because the antigen-presenting capacity was not influenced by the presence or absence of E molecules, class II A molecules can be attributed to this event. The importance of mixed haplotype $\alpha/\beta$ heterodimers also was supported by findings of Gotoh *et al.* (7), in

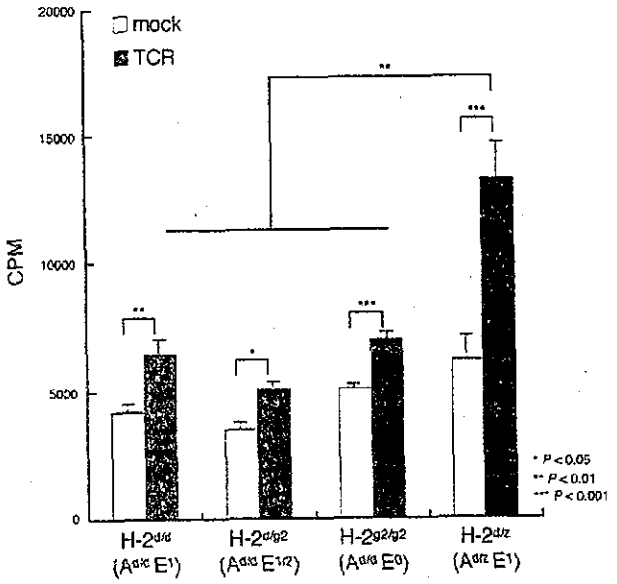


Fig. 4. The potential for chromatin presentation by CD11c-positive splenic cells from (NZB × NZW)$F_1$ mice with different H-2 haplotypes. Splenic T cells from (NZB × NZW)$F_1$ mice transfected with chromatin-specific TCR $V_\alpha$ and $V_\beta$ or with vector alone (mock) were cocultured with CD11c-positive splenic DCs obtained from $F_1$ mice with different H-2 haplotypes, in the presence of chromatin, and T cell proliferative responses were compared. DCs from all these $F_1$ mice induced significant levels of chromatin-specific T cell responses; however, the potential of DCs for chromatin presentation was significantly higher in wild-type H-$2^{d/z}$ $F_1$ mice than that in other $F_1$ groups. Means and SE of three experiments are shown.

which the $A\alpha^d\beta^z$-restricted self-reactive T cell clone isolated from (NZB × NZW)$F_1$ mice had a potential to induce IgG anti-DNA antibodies *in vivo* (8). These $F_1$-unique mixed haplotype class II $\alpha/\beta$ heterodimers also may be involved in the aberrant selection of self-reactive T cells in the thymus. Based on studies by Braunstein and Germain (41), the assembly of $A\alpha$ and $A\beta$ chains of different haplotypes is under serious pairing restrictions. Thus, low expression levels of these heterodimers in the thymic epithelial cells may allow $\alpha/\beta$ heterodimer-restricted self-reactive T cells to escape from negative selection in the thymus.

In contrast to A molecules, the mixed-haplotype E molecules are not formed in most of the H-2 heterozygotes, because $E\alpha$ chains are usually nonpolymorphic (42). However, $E\alpha^z$ is unique among the $E\alpha$ chains of other haplotypes and has two amino acid substitutions in the $\alpha$1 domain (43, 44). Thus, $F_1$ unique E molecules can be formed in H-$2^{d/z}$ $F_1$ mice. In this context, Nygard *et al.* (45) proposed the possible preferential formation of $E\alpha^d\beta^z$ mixed haplotype molecules and their involvement in the promotion of $F_1$ disease. However, evidence indicated that $E\alpha^d\beta^z$ molecules are protective rather than promoting (20).

The protective mechanism by E molecules remains elusive; however, several possibilities are suggested. First is the E-mediated clonal deletion model of self-reactive T cells in the thymus. It has been shown that T cells bearing TCR $V_\beta5$, $V_\beta11$, $V_\beta12$, and $V_\beta17a$ are eliminated in E-positive strains of mice (34–36), although the extent of negative selection is influenced by background genes (46–48). In this context, there are reports indicating that no clear-cut difference in the expression of TCR $V_\beta$ repertoire was observed between $E^+$ and $E^-$ transgenic NOD (16) as well as collagen-induced arthritis-susceptible B10.RQB3 mice (49), although the E transgene protected against the disease. Hence, the clonal deletion hypothesis for E-mediated protection of autoimmune disease has been dismissed in cases of these models. In the (NZB × NZW)$F_1$ genetic background, however, CD4 T cell repertoires bearing TCR $V_\beta11$ and $V_\beta12$ were significantly negatively selected in mice expressing E molecules. Thus, clonal deletion remains one possible mechanism at work in our mouse models.

Second is the determinant capture model. In $Ea^d$-transgenic BXSB mice, transgene-derived $E\alpha^d$ peptides bind to $A^b$ molecules, possibly decreasing the use of A molecules for presentation of pathogenic self-peptides (18). Rudensky *et al.* (50) showed evidence for the binding of $E\alpha^d$ peptides to $A^b$ molecules in a sequence analysis of peptides derived from the cell surface. This mechanism may be involved in the E-transgene-mediated protection of the collagen-induced arthritis model of $E\beta$-deficient B10.RQB3 mice (51, 52). However, such a mechanism may not be operative in our model, because the potential for chromatin presentation by $CD11C^+$ DCs was not affected by E molecules expressed in $A^{d/d}$ $F_1$ mice. This notion is in agreement with the finding by Nakano *et al.* (53) that antigen-presenting cells from both $E^+$ and $E^-$ NOD mice can similarly stimulate diabetogenic T cells.

Third is the cytokine balance model. Hanson *et al.* (19) proposed that E molecule-mediated Th1/Th2 cytokine imbalance is one possible mechanism for the disease protection in $E\alpha^d$-transgenic NOD mice. Indeed, there is evidence that the differential MHC class II expression on antigen-presenting cells mediated by class II promoter polymorphism exerts a codominant effect on the Th1/Th2 cytokine balance (54, 55). In our preliminary studies, however, there was no clear difference in the potential of anti-CD3-stimulated T cells to produce IL-4 and IFN-$\gamma$ between $E^+$ and $E^-$ $A^{d/d}$ $F_1$ mice (data not shown).

An alternative is the signal transducer competition model, in which B cells may be the major cellular sites of E molecule-mediated autoimmune protection. Lang *et al.* (56) reported that antigen stimulation by means of the B cell antigen receptor on resting B cells induces association of MHC class II molecules with B cell antigen receptor-derived Ig-$\alpha$/Ig-$\beta$ heterodimers, which function as signal transducers on class II aggregation by the TCR. Because both A and E molecules physiologically associate with Ig-$\alpha/\beta$ heterodimers (56), when self-reactive B cells were stimulated by A-restricted T helper cells plus self-peptides, E molecules possibly associate competitively with Ig-$\alpha/\beta$ heterodimers. Hence, activation signals should be lower in $E^+$ than in $E^-$ B cells. This idea well explains the observed dose dependency of E-mediated protection of SLE seen in the present studies.

Wild-type H-$2^{d/z}$ $F_1$ mice develop severe SLE, although they do express intact E molecules. This finding is in striking contrast to findings in H-$2^{d/d}$ $F_1$ mice that develop the disease only when lacking E molecules. Two mechanisms are thought to be involved. First, compared with H-$2^{d/d}$ $F_1$, the self-antigen-presenting capacity of DCs in H-$2^{d/z}$ $F_1$ is much higher, so that effects of E molecules may be insufficient for suppression. Alternatively, although not mutually exclusive, generation of H-$2^{d/z}$ $F_1$-unique self-reactive T cells restricted to haplotype-mismatched $A\alpha/\beta$ heterodimers in the thymus, as discussed above, may play a role in an E molecule-independent manner.

Taken collectively, our mouse models may provide means for further clarification of molecular mechanisms involved in the positive and negative regulation of autoimmune disease mediated by class II A and E molecules. Studies on the suppressive effect of E molecules are of particular importance, because one can apply this knowledge to future prophylactic and therapeutic approaches to autoimmune diseases.

We thank Prof. S. Matsushita (Saitama Medical School, Saitama, Japan) for helpful discussion and M. Ohara (Fukuoka, Japan) for language assistance. This work was supported in part by a Grant-in-Aid for

Scientific Research (B) for Scientific Research on Priority Areas and for Center of Excellence Research from the Ministry of Education, Science, Technology, Sports, and Culture of Japan and a grant from the Organization for Pharmaceutical Safety and Research (Japan).


1. Tsao, B. P. (2002) in *Dubois' Lupus Erythematosus*, eds. Wallace. D. J. & Hahn. B. H. (Lippincott Williams & Wilkins, Philadelphia), pp. 97–119.
2. Hirose, S., Nagasawa. R., Sekikawa, I., Hamaoki, M., Ishida, Y., Sato. H. & Shirai. T. (1983) *J. Exp. Med.* **158**, 228–233.
3. Hirose, S., Ueda. G., Noguchi. K., Okada. T., Sekigawa, I., Sato, H. & Shirai, T. (1986) *Eur. J. Immunol.* **16**, 1631–1635.
4. Kotzin, B. L. & Palmer, E. (1987) *J. Exp. Med.* **165**, 1237–1251.
5. Hirose, S., Kinoshita, K., Nozawa, S., Nishimura. H. & Shirai, T. (1990) *Int. Immunol.* **2**, 1091–1095.
6. Kono. D. H., Burlingame. R. W., Owens. D. G., Kuramochi. A., Balderas. R. S., Balomenos, D. & Theofilopoulos, A. N. (1994) *Proc. Natl. Acad. Sci. USA* **91**, 10168–10172.
7. Gotoh, Y., Takashima, T., Noguchi. K., Nishimura. H., Tokushima, M., Shirai. T. & Kimoto. M. (1993) *J. Immunol.* **150**, 4777–4787.
8. Tokushima, M., Koarada, S., Hirose, S., Gotoh, Y., Nishimura. H., Shirai, T., Miyake. K. & Kimoto. M. (1994) *Immunology* **83**, 221–226.
9. Murphy, E. D. & Roths. J. B. (1979) *Arthritis Rheum.* **22**, 1188–1194.
10. Merino, R., Fossati. L., Lacour. M., Lemoine, R., Higaki, M. & Izui, S. (1992) *Eur. J. Immunol.* **22**, 295–299.
11. Merino, R., Iwamoto. M., Fossati, L., Muniesa. P., Araki. K., Takahashi, S., Huarte. J., Yamamura, K. I., Vassalli, J. D. & Izui, S. (1993) *J. Exp. Med.* **178**, 1189–1197.
12. Hattori. M., Buse, J., Jackson. R., Glimcher, L., Dorf, M., Minami. M., Makino, S., Moriwaki. K., Kuzuya. H., Imura, H., *et al.* (1986) *Science* **231**, 733–735.
13. Acha-Orbea. H. & McDevitt. H. (1987) *Proc. Natl. Acad. Sci. USA* **84**, 2435–2439.
14. Nishimoto. H., Kikutani, H., Yamamura. K. & Kishimoto, T. (1989) *Nature* **328**, 432–434.
15. Lund, T., O'Reilly. L., Hutchings, P., Kanagawa, O., Simpson. E., Gravely, R., Chandler, P., Dyson, J., Picard, J., Edwards, A., *et al.* (1990) *Nature* **345**, 727–729.
16. Bohme, J., Schuhbaur, B., Kanagawa. O., Benoist, C. & Mathis, D. (1990) *Science* **249**, 293–295.
17. Labrecque. N., Madsen, L., Fugger. L., Benoist, C. & Mathis, D. (1999) *Immunity* **11**, 515–516.
18. Iwamoto. M., Ibnou-Zekri. N., Araki, K. & Izui. S. (1996) *Eur. J. Immmunol.* **26**, 307–314.
19. Hanson, M. S., Cetkovic-Cvrlje, M., Ramiya, V. K., Atkinson, M. A., Maclaren, N. K., Singh, B., Elliott, J. F., Serreze, D. V. & Leiter, E. H. (1996) *J. Immunol.* **157**, 1279–1287.
20. Hirose, S., Zhang, D., Nozawa, S., Nishimura. H. & Shirai, T. (1994) *Immunogenetics* **40**, 150–153.
21. Figueroa, F., Tewarson, S., Neufeld, E. & Klein, J. (1982) *Immunogenetics* **15**, 431–436.
22. Jongeneel, C. V., Acha-Orbea, H. & Blankenstein, T. (1990) *J. Exp. Med.* **171**, 2141–2146.
23. Jacob, C. O., Hwang, F., Lewis, G. D. & Stall, A. M. (1991) *Cytokine* **3**, 551–561.
24. Fujimura, T., Hirose, S., Jiang, Y., Kodera, S., Ohmuro. H., Zhang, D., Hamano, Y., Ishida, H., Fukukawa, S. & Shirai, T. (1998) *Int. Immunol.* **10**, 1467–1472.
25. Knight, J. G. & Adams, D. D. (1978) *J. Exp. Med.* **147**, 1653–1660.
26. Bates. D. L., Butler, P. J., Pearson. E. C. & Thomas, J. O. (1981) *Eur. J. Biochem.* **119**, 469–476.
27. Mohan, C., Adams. S., Stanik, V. & Datta, S. K. (1993) *J. Exp. Med.* **177**, 1367–1381.
28. Kaliyaperumal, A., Mohan. C., Wu, W. & Datta, S. K. (1996) *J. Exp. Med.* **183**, 2459–2469.
29. Fujio, K., Misaki, Y., Setoguchi, K., Morita, S., Kawahata, K., Kato, I., Nosaka, T., Yamamoto, K. & Kitamura, T. (2000) *J. Immunol.* **165**, 528–532.
30. Zufferey, R., Donello, J. E., Trono, D. & Hope, T. J. (1999) *J. Virol.* **73**, 2886–2892.
31. Morita, S., Kojima, T. & Kitamura, T. (2000) *Gene Ther.* **7**, 1063–1066.
32. Lilly, F. & Klein, Y. (1973) *Transplantation* **16**, 530–532.
33. Ishikawa, S., Akakura, S., Abe, M., Terashima, K., Chijiiwa, K., Nishimura, H., Hirose, S. & Shirai, T. (1998) *J. Immunol.* **161**, 1267–1273.
34. Kappler, J. W., Roehm, N. & Marrack, P. (1987) *Cell* **49**, 273–280.
35. Bill, J., Appel, V. & Palmer, E. (1988) *Proc. Natl. Acad. Sci. USA* **85**, 9184–9188.
36. Bill, J., Kanagawa, O., Woodland, D. L. & Palmer, E. (1989) *J. Exp. Med.* **169**, 1405–1419.
37. Shi. Y., Kaliyaperumal, A., Lu. L., Southwood, S., Sette, A., Michaels, M. A. & Datta, S. K. (1998) *J. Exp. Med.* **187**, 367–378.
38. Fujio. K., Okamoto, A., Tahara, H., Abe, M., Jiang, Y., Kitamura, T., Hirose, S. & Yamamoto, K. (2004) *J. Immunol.* **173**, 2118–2125.
39. Jacob. C. O. & McDevitt, H. O. (1988) *Nature* **331**, 356–358.
40. La Cava, A., Balasa, B., Good, A., van Gunst, K., Jung, N. & Sarvetnick, N. (2001) *J. Immunol.* **167**, 1066–1071.
41. Braunstein, N. S. & Germain, R. N. (1987) *Pro. Natl. Acad. Sci. USA* **84**, 2921–2925.
42. Mathis, D. J., Benoist, C. O., Williams, V. E., II, Kanter, M. R. & McDevitt, H. O. (1983) *Cell* **32**, 745–754.
43. Sciffenbauer, J., McCarthy, D. M., Nygard, N. R., Woulfe, S. L., Didier, D. K. & Schwartz, B. D. (1989) *J. Exp. Med.* **170**, 971–984.
44. Ogawa, S., Nishimura, H., Awaji, M., Nozawa, S., Hirose, S. & Shirai, T. (1990) *Immunogenetics* **32**, 63–67.
45. Nygard, N. R., McCarthy, D. M., Schiffenbauer, J. & Schwartz, B. D. (1993) *Immunol. Today* **14**, 53–56.
46. Kappler, J. W., Staerz, U., White, J. & Marrack, P. (1987) *Nature* **332**, 35–40.
47. MacDonald, H. R., Schneider, R., Lees, R. K., Howe, R. C., Acha-Orbea, H., Festenstein, H., Zinkernagel, R. M. & Hengartner, H. (1988) *Nature* **332**, 40–45.
48. Pullen, A. M., Marrack, P. & Kappler, J. W. (1988) *Nature* **335**, 796–801.
49. Gonzalez-Gay, M. A., Nabozny, G. H., Bull, M. J., Zanelli, E., Douhan, J., III, Griffiths, M. M., Glimcher, L. H., Luthra, H. S. & David, C. S. (1994) *J. Exp. Med.* **180**, 1559–1564.
50. Rudensky, A. Y., Preston-Hurlburt, P., Hong, S. C., Barlow, A. & Janeway, C. A., Jr. (1991) *Nature* **353**, 622–627.
51. Gonzalez-Gay, M. A., Zanelli, E., Krco, C. J., Nabozny, G. H., Hanson, J., Griffiths, M. M., Luthra, H. S. & David, C. S. (1995) *Immunogenetics* **42**, 35–40.
52. Gonzalez-Gay, M. A., Zanelli, E., Khare, S. D., Krco, C. J., Griffiths, M. M., Luthra, H. S. & David, C. S. (1996) *Immunogenetics* **44**, 377–384.
53. Nakano, N., Kikutani, H., Nishimoto, H. & Kishimoto, H. (1991) *J. Exp. Med.* **173**, 1091–1097.
54. Guardiola, J., Maffei, A., Lauster, R., Mitchison, N. A., Accolla, R. S. & Sartoris. S. (1996) *Tissue Antigens* **48**, 615–625.
55. Baumgard. M., Moos, V., Schuhbauer, D. & Müller, B. (1998) *Proc. Natl. Acad. Sci. USA* **95**, 6936–6940.
56. Lang, P., Stolpa. J.C., Freiberg, B. A., Crawford. F., Kappler, J., Kupfer, A. & Cambier, J. C. (2001) *Science* **291**, 1537–1540.

Available online at www.sciencedirect.com
SCIENCE DIRECT®
Analytical Biochemistry 337 (2005) 316–324
ANALYTICAL BIOCHEMISTRY
www.elsevier.com/locate/yabio

# Isolation and mass spectrometry characterization of molecular species of lactosylceramides using liquid chromatography-electrospray ion trap mass spectrometry

Naoko Kaga[a], Saiko Kazuno[a], Hikari Taka[a], Kazuhisa Iwabuchi[b,c], Kimie Murayama[a,*]

[a] *Division of Proteomics and Biomolecular Science, BioMedical Research Center, Juntendo University Graduate School of Medicine, Tokyo 113-8421, Japan*
[b] *Institute for Environmental and Gender-Specific Medicine, Juntendo University Graduate School of Medicine, Tokyo 113-8421, Japan*
[c] *Laboratory of Biochemistry, Juntendo University School of Healthcare and Nursing, Chiba, Japan*

Received 27 September 2004
Available online 2 December 2004

**Abstract**

Reverse-phase liquid chromatography/electrospray ion trap mass spectrometry (LC-ESI-$MS^n$) was established for identification of the molecular species of lactosylceramides. Lactosylceramides derived from porcine blood cells were separated on a CapcellPak $C_8$ column using a mixture of methanol and 1 mM ammonium formate from the $C_{16}$ to $C_{26}$ fatty acyl chains based on the length of total carbon chains and the nature of sphingoid bases ($w^n$) and fatty acyl chains ($Y^t_0 - w^n$) was identified by $MS^3$ as their $[M + H]^+$ ions. The same number of fatty acyl moieties appeared in the order of unsaturated, (2-)hydroxylated, and saturated components. The molecular species of lactosylceramides derived from porcine blood cells totaled more than 33 and included mainly $C_{24:0}$-$d_{18:1}$, $Ch_{24:0}$-$d_{18:1}$, $Ch_{24:1}$-$d_{18:1}$, $C_{24:1}$-$d_{18:1}$, and $C_{22:0}$-$d_{18:1}$ in addition to 28 minor species from $C_{16:0}$ to $C_{26:0}$ fatty acyl moieties. The molecular species of lactosylceramides in the membrane microdomain fraction of HL-60 cells (70% were differentiated into macrophage-lineage cells) were identified as $C_{24:0}$-$d_{18:1}$, $C_{24:1}$-$d_{18:1}$, $C_{22:0}$-$d_{18:1}$, $C_{16:0}$-$d_{18:1}$, and more than 21 other minor species. Our results suggest that reverse-phase LC-ESI-$MS^n$ is a useful and simple method for identification of lactosylceramide molecular species.


*Keywords:* Lactosylceramide; Molecular species; Fatty acyl chain moiety; Long-chain base moiety; LC-ESI-$MS^n$

Studies on molecular membrane biology have focused on the dynamics of cellular proteins and the lipid microenvironment at the cell surface [1]. It is known that glycosphingolipids play important roles in cell–cell interaction, recognition, transmembrane signaling, and cellular growth and differentiation in animal cells [2]. These compounds self-aggregate easily based on their nature and cluster with sphingomyelin with or without cholesterol and various signal transducer molecules to form various types of microdomains called "lipid-raft" at plasma membrane [3–6]. Although the lipid composition of the rafts in different cells is not clear, lactosylceramides are known to localize with "sphingolipid-sterol rafts" and trigger raft-related signal transduction processes. In neutrophils, lactosylceramide-enriched microdomains on the cell surface coupled with tyrosine protein kinase LYN (Lyn)[1] induce the activation of Lyn via lactosylceramides and lead to superoxide generation [3].

To understand the biological activity and physical behavior of lactosylceramides, it is important to deter-

* Corresponding author. Fax: +81 3 3818 6330.
*E-mail address:* murayama@med.juntendo.ac.jp (K. Murayama).

[1] *Abbreviations used:* Lyn, tyrosine protein kinase LYN; FAB, fast atom bombardment; CAD, collisional-activated dissociation; CID, collision-induced dissociation; ESI, electrospray ionization; APCI, atmospheric pressure chemical ionization; DFP, diisopropylphosphorofluoridate; SIM, single ion monitoring; 3D, three-dimensional.

0003-2697/$ - see front matter © 2004 Elsevier Inc. All rights reserved.
doi:10.1016/j.ab.2004.11.003

mine their structural heterogeneity. Lactosylceramides contain lactose and a ceramide moiety. Various classes of the sphingoid base have been identified, such as the dihydro type (sphinganine), the additional hydroxyl group type (phytosphingosine), and the 2-amino-4-ene-1,3-diol type with 14–22 carbon chains (sphingenine). The commonest type in animal tissues is $C_{18}$ sphingenine ($-d_{18:1}$). In addition, significant variation can also occur in fatty acyl moiety with regard to chain length, unsaturation, and hydroxylation. Lactosylceramides containing saturated fatty acyl chains display relatively high thermotropic and pressure-induced transition, but the introduction of a single *cis* double bond into the fatty acyl chains markedly reduce these properties, especially when the double bonds are located near the middle of the fatty acyl chain [6].

Mass spectrometry (MS) is a powerful tool for lipid structure analysis. Several methods incorporating tandem MS for identification of intact ceramides and neutral sphingolipids such as glucosyl- and lactosylceramides have been published. In early 1990s, Costello and Vath [7] used fast atom bombardment tandem mass spectrometry (FAB-MS/MS) and reported valuable data about the structure of glycosphingolipids, such as the molecular weight of fatty acyl chain and sphingoid base, by analyzing the MS/MS spectra of $[M+H]^+$ and $[M-H]^-$ ions. Ann and Adams [8,9] and Duarte et al. [10] also reported that, in the presence of alkaline metal, $[M+\text{metal}]^+$ ions were formed with ceramides and glucosylceramides and these showed a much higher sensitivity than the $[M+H]^+$ ions. In addition, they provided more informative MS/MS spectra for the location of double bonds at high-energy CAD, by using charge remote cleavage. At present, electrospray ionization tandem mass spectrometry (ESI-MS/MS) and atmospheric pressure chemical ionization tandem mass spectrometry (APCI-MS/MS) are used for determination of the structure of intact ceramides and lactosylceramides with low-energy CID [11–13] or high-energy CID [14]. Lee et al. [15] and Pettus et al. [16] reported analysis of the molecular species of ceramides by reverse-phase LC-ESI/MS/MS and normal-phase LC-APCI/MS/MS, respectively.

We report here the design of a simple and useful method for separation and $MS^n$ characterization of molecular species of lactosylceramides using reverse-phase HPLC-ESI ion trap mass spectrometry.

## Materials and methods

### *Materials*

Lactosylceramide derived from porcine blood cells was purchased from Matreya (Pleasant Gap, PA). The synthetic lactosylceramide for $C_{24:1}$-$d_{18:1}$ was provided by Professor Sandro Sonnino (Center of Excellence on Neurodegenerative Diseases, Department of Medical Chemistry, Biochemistry and Biotechnology, University of Milan, Italy). All reagents used in this study were of the highest grade, especially those used for HPLC, spectrometry, and amino acid analysis. Chloroform, acetone, sodium chloride, methanol, ethylenediaminetetraacetic acid (EDTA), Triton X-100, Tris–HCl, vitamin $D_3$, and diisopropylphosphorofluoridate (DFP) were purchased from Wako Pure Chemical Industries (Osaka, Japan). Lithium chloride anhydrous and ethylene glycol bis (β-aminoethyl ether)-*N,N,N′,N′*-tetraacetic acid (EGTA) were obtained from Nacalai Tesque (Kyoto, Japan). Ammonium acetate, ammonium formate, and primulin were from Sigma–Aldrich (St. Louis, MO). Complete is a product of Roche (Switzerland). Ultrapure water was prepared using the Millipore Milli-Q purification system (Bedford, MA).

### *Mass spectrometric analysis*

All analyses were performed in positive mode using a LCQ DECA XP ion trap mass spectrometer (Thermo Electron, San Jose, CA) with a conventional electrospray ionization source.

### *Infusion-ESI-$MS^n$ analysis*

Lactosylceramide at a concentration of 5–10 ng/μl was dissolved in methanol with or without alkaline and ammonium salts (1 mM LiCl, 1 mM NaCl, and 10 mM ammonium acetate). Sample solution was directly infused at a rate of 3–5 μl/min into the ESI source without separation of the molecular species of lactosylceramides. The temperature of the ion transfer tube was set at 150–400 °C. The spray voltage was set at 5 kV and the nitrogen sheath gas pressure used was 10 U. In $MS^n$ ($n = 2$–4) analysis, the collision energy was fixed at 100%.

*HPLC-ESI-$MS^n$ analysis.* Reverse-phase HPLC was carried out with the Magic2002 system (Michrom BioResources, Auburn, CA). The column was Capcellpak $C_8$ UG120, 1.0 mm ID × 150 mm (Shiseido Fine Chemicals, Tokyo). The mobile phases were as follows: solvent A was 1 mM ammonium formate in methanol:water (76:24 v/v) and solvent B was 1 mM ammonium formate in methanol:water (96:4 v/v). The elution program was isocratic elution with 80% B for 5 min, increase to 95% B, and then hold for 30 min. The flow rate was 50 μl/min. The HPLC was joined to the mass spectrometer, LCQ DECA XP. The MS conditions were as follows: ion transfer tube temperature 250 °C, spray voltage 5 kV, sheath gas pressure 20 U. $MS^n$ ($n = 4$) analysis was performed on data-dependent experiments (DDE) with collision energy 80%.

*Identification of molecular species of lactosylceramides in the membrane microdomain fraction of HL-60 cells*

*Fractionation of the membrane microdomain fraction of HL-60 cells.* Cells of the myeloid leukemia cell line HL-60 were maintained in RPMI 1640 medium supplemented with 10% fetal bovine serum. HL-60 cells ($2 \times 10^8$ cells) were treated with active form vitamin $D_3$ (final concentration, 100 nM) for 5 days. Flow cytometric analysis using anti-CD11b antibody was performed as described previously [3]. Iwabuchi and Nagaoka [3] indicated that about 70% of the cells were differentiated into macrophage-lineage cells. Cells were resuspended in relaxation buffer (10 mM 1,4 piperazinedichanesulfonic acid, 100 mM KCl, 3 mM NaCl, 3.5 mM $MgCl_2$, and 1 mM ATP, pH 7.4) containing a mixture of protease inhibitors (1 mM phenylmethylsulfonyl fluoride, 0.4 μM aprotinin, 10 μM E-64, 20 μM leupeptin, 10 μM bestatin, 5 μM *N*-acetyl-Leu-Leu-Met-al, and 2 μM pepstatin) and disrupted by nitrogen cavitation ($N_2$ for 20 min at 350 psi). Disrupted cells were dropped gradually into EGTA solution (final concentration, 1.25 mM). All manipulations were carried out at 4 °C. The plasma membrane was fractionated after sequential centrifugation; 500*g* at 4 °C for 10 min, 8500*g* for 20 min, and 200,000*g* for 1 h. This fraction was suspended in TNE-T buffer [1% Triton X-100, 10 mM Tris–HCl (pH 7.5), 150 mM Nacl, 1 mM DFP] containing 1/20 Complete.

*Extraction of crude lactosylceramides.* The crude lipids in the membrane microdomain fraction were extracted with a chloroform:methanol mixture (2:1 v/v). A fifth of them (20 μl/100 μl crude lipids) were separated on a 10 × 10-cm high-performance thin-layer chromatography (HPTLC) plate (Merck, Rahway, NJ) with chloroform/methanol/water 65:25:4 (v/v/v). After development, lactosylceramides were visualized using primulin reagent (0.03% in 80% acetone) under ultraviolet light. Lactosylceramide-containing bands were scratched out from the plate and extracted with chloroform/methanol (2:1 v/v). After drying, lactosylceramides were dissolved in 20 μl of methanol and 4 μl of the solution was loaded on the column for LC-ESI-$MS^n$ analysis. Finally, lactosylceramides from HL-60 ($8 \times 10^6$ cells) were analyzed.

## Results and discussion

*Effects of salts and temperature on ionization of synthetic lactosylceramide at $C_{24:1}$-$d_{18:1}$*

To compare the effects of salts and ion transfer tube temperature on ionization of lactosylceramide by infusion analysis, synthetic lactosylceramide at $C_{24:1}$-$d_{18:1}$ was dissolved in methanol with/without 1 mM LiCl, NaCl, or 10 mM ammonium acetate at 5 ng/μl and analyzed with the ion trap mass spectrometer. In salt-free condition, lactosylceramide at $C_{24:1}$-$d_{18:1}$ did not produce the $[M + H]^+$ ion at 400 °C, but the $[M + Na]^+$ ion, which was produced from concomitant sodium in the sample or reagents, was stable.

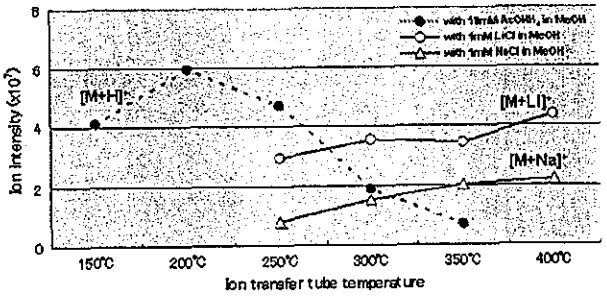


Fig. 1. Effects of salts and temperature on ionization of lactosylceramide by infusion analysis. Synthetic lactosylceramide of $C_{24:1}$-$d_{18:1}$ was dissolved in methanol containing each salt at 5 ng/μl concentration. The flow rate was 3 μl/min.

The addition of 1 mM NaCl to lactosylceramide markedly increased the amount of $[M + Na]^+$ ion at 400 °C (Fig. 1). On the other hand, the amount of $[M + Li]^+$ ion was twice as much as that of $[M + Na]^+$ ion at the same temperature. However, the addition of 10 mM ammonium acetate tended to produce the $[M + H]^+$ ion at 200 °C. The higher temperature (400 °C) for the $[M + H]^+$ ion was associated with the generation of dehydrated ion and resulted in a complex spectrum.

On the other hand, the $[M + Na]^+$ ion of lactosylceramide could not be produced at 200 °C. The optimal temperature of the ion transfer tube was 400 °C for the $[M + metal]^+$ ion and 200 °C for the $[M + H]^+$ ion.

*$MS^n$ analysis of $[M + Li]^+$ and $[M + H]^+$ ion to characterize fatty acyl chain and long-chain base moiety*

We performed $MS^n$ analysis for $[M + Li]^+$ and $[M + H]^+$ ion of synthetic lactosylceramide ($C_{24:1}$-$d_{18:1}$) at optimal temperature (Fig. 2). In $MS^n$ analysis for $[M + Li]^+$ ion, following the loss of one or two hexose(s) [$Y_1$,$Y_0$] and water [represented as ′, ″], a HCHO was eliminated to form [$a_2$] ion[11] on the $MS^2$/$MS^3$ spectra (Fig. 2A). [$Y_0$] and [$a_2$] ions were extremely stable at 400 °C and no further cleavage occurred on the $MS^4$ spectrum. We could not obtain information on the fatty acyl chain and long-chain base, even though the dissociation energy increased up to 100%. However, lactosylceramides containing 2-hydroxy fatty acyl chain underwent marked cleavage of the N–CO bond on the $MS^3$ spectrum and characterized the fatty acyl chain (data not shown).

On the other hand, in $MS^n$ analysis of $[M + H]^+$ ion, the loss of two hexoses and water [$Y'_0$] on the $MS^2$ spec-

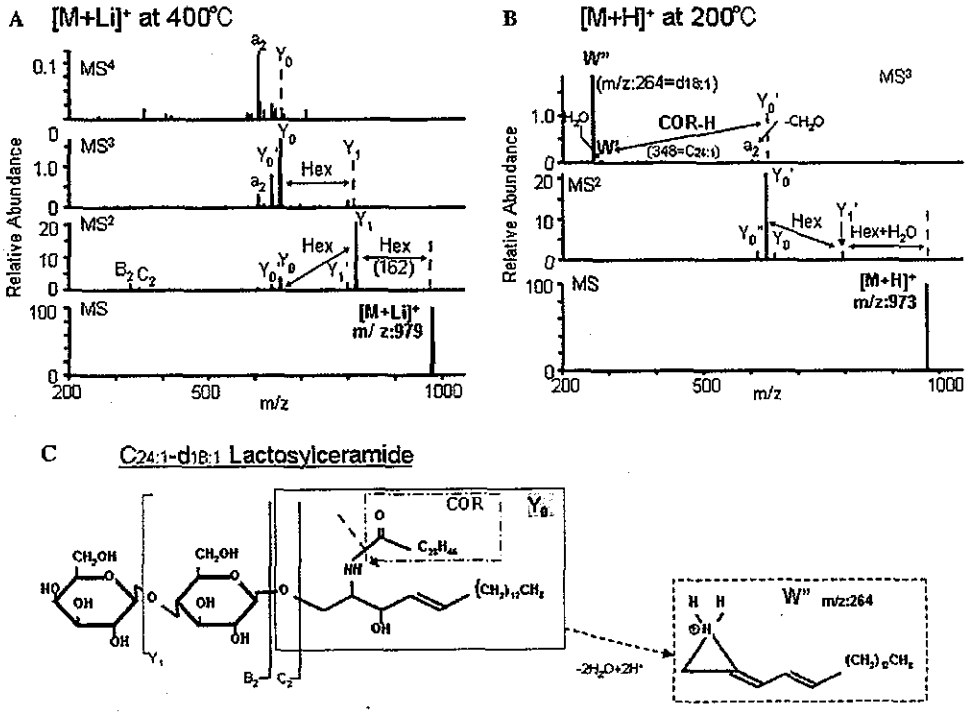


Fig. 2. $MS^n$ spectra of synthetic lactosylceramide of $C_{24:1}$-$d_{18:1}$ using ESI-ion trap mass spectrometer. (A) $MS^n$ spectra ($n = 1$–4) of the lithiated molecular ion $[M + Li]^+$ with 1 mM LiCl in methanol at 400 °C. (B) $MS^n$ spectra ($n = 1$–3) of the protonated molecular ion $[M + H]^+$ with 10 mM ammonium acetate in methanol at 200 °C. The collision energy was 100%. (C) Predicted cleavage scheme for lactosylceramide shows hexose (*Hex*), loss of hexoses ($Y_0$), long-chain base (w series), and fatty acyl chain (COR-H).

trum was associated with cleavage of the immediate N–CO bond on the $MS^3$ spectrum and identification of a long-chain base (w ion series) and a fatty acyl chain ($[Y'_0 - w' = COR - H]$) [7] (Fig. 2B). On the $MS^3$ spectrum, *m/z* 264 was found as a fragment ion of $Y'_0$ regarded as w″ ion, which was assigned to $d_{18:1}$, and the fatty acyl chain was identified as $C_{24:1}$ [7].

The use of sequential $MS^n$ analysis allowed us to obtain the dissociation patterns of a single ion in multiple steps when that was compared with MS/MS analysis using FAB-MS or triple stage ESI/MS. The patterns were simple, thus allowing speculation on the structure of the molecular species.

### *Molecular species of lactosylceramides derived from porcine blood cells using infusion analysis*

The molecular species of lactosylceramides derived from porcine blood cells were determined using infusion analysis. The MS spectrum for those ionized with 1 mM ammonium acetate is shown in Fig. 3.

The molecular species of lactosylceramides comprised more than 14 different structures from $C_{16:0}$-$d_{18:1}$ to $Ch_{26:1}$-$d_{18:1}$. The main species were $C_{22:0}$-$d_{18:1}$, $C_{24:1}$-$d_{18:1}$, $C_{24:0}$-$d_{18:1}$, $Ch_{24:1}$-$d_{18:1}$, and $Ch_{24:0}$-$d_{18:1}$, similar to the results of a previous study [11].

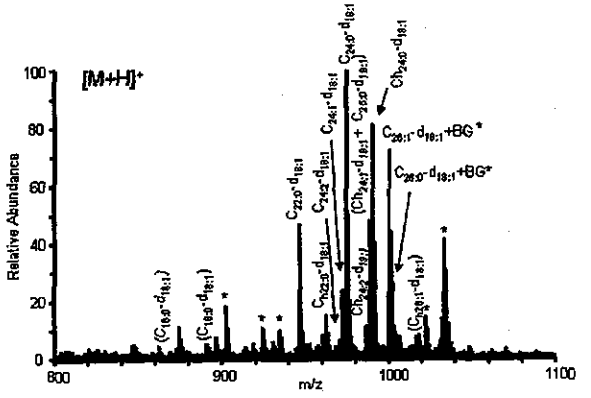


Fig. 3. ESI-MS spectrum of lactosylceramides derived from porcine blood cells ionized with ammonium salt using infusion analysis. Lactosylceramides were dissolved in 10 mM ammonium acetate in methanol at 10 ng/μl concentration, the ion transfer tube was set at 200 °C. The molecules were detected as protonated molecular ions, $[M + H]^+$. The parenthetic formulae of lactosylceramides were characterized using other methods. *Represent those revealing background ions from the reagents. Some ions at *m/z* 1001 and 1003 were similar to the $[M + H]^+$ ions of $C_{26:1}$-$d_{18:1}$ and $C_{26:0}$-$d_{18:1}$ but they were distinguished from the background ions on $MS^n$ analysis.

The use of infusion analysis was associated with one problem; it was impossible to distinguish fatty acyl chains between Cn:x and $Ch(n-1):(x+1)$ by $MS^n$

analysis because of the same value of COR-H at *m/z* 364 for $C_{25:0}$ and $Ch_{24:1}$ fatty acyl chains.

### *LC-ESI-MS for classification of molecular species of lactosylceramides by single ion monitoring (SIM) mode*

The molecular species of lactosylceramides were separated on a $C_8$ reverse-phase column and identified using the LCQ ion trap mass spectrometer by characterizing their fatty acyl chain and long-chain base moieties by $MS^n$ analysis. Fig. 4A shows the three-dimensional (3D) HPLC mass chromatogram of 200 ng of total lactosylceramides derived from porcine blood cells. The abscissa, ordinate, and *z* axis indicate the retention time, relative abundance of ions, and *m/z*, respectively.

In the case of LC-MS, we used methanol containing 1 mM ammonium formate as a solvent because the formate produced stable and abundant $[M + H]^+$ ions and $[M + Na]^+$ ions were minimum as contaminants.

It was assumed that the long chain base of lactosylceramides has $d_{18:1}$ sphingenine, because this is the commonest type in animal tissues [17]. In Figs. 4B–E, $[M + H]^+$ ions of lactosylceramide molecular species were monitored in the SIM mode for classification according to fatty acyl carbon chain into (B) straight saturated (n:0), (C) straight unsaturated (n:1), (D) saturated and hydroxylated (hn:0), and (E) unsaturated and hydroxylated (hn:1) fatty acyl chains. We also monitored $d_{18:0}$ sphinganine, but no significant peak of lactosylceramides appeared in porcine blood cells (data not

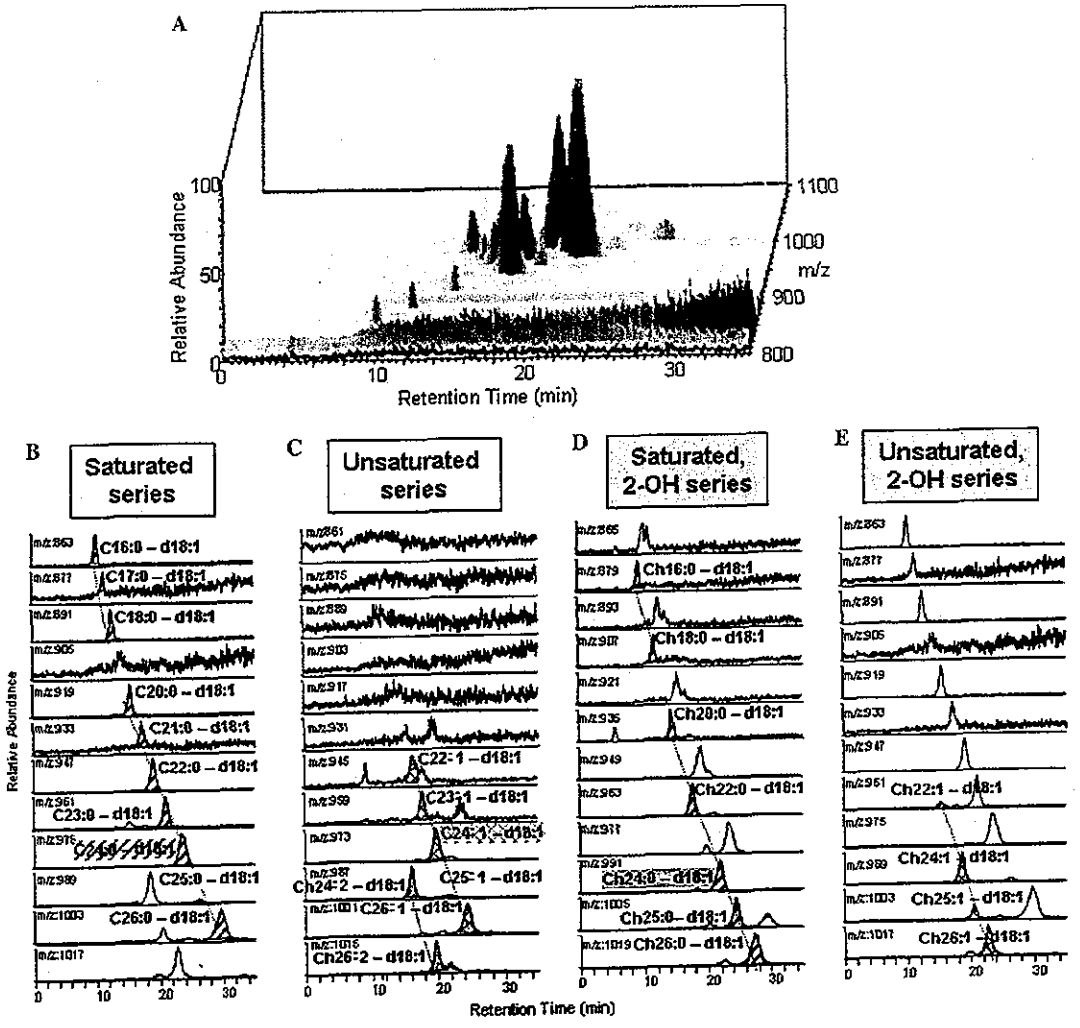


Fig. 4. Three-dimensional HPLC mass chromatogram of lactosylceramides derived from porcine blood cells and selected ion monitoring (SIM) chromatograms. (A) 3D-HPLC-ESI/MS chromatogram of 200 ng of lactosylceramide. SIM chromatograms monitored the $[M + H]^+$ ions of lactosylceramide molecular species classified according to fatty acyl carbon chain into (B) straight saturated (n:0), (C) straight unsaturated (n:1), (D) saturated and hydroxylated (hn:0), and (E) unsaturated and hydroxylated (hn:1).

shown). In the straight saturated molecular species (Fig. 4B), the retention time of lactosylceramides correlated with the length of their fatty acyl chain from 10 min for $C_{16:0}$ to 30 min for $C_{26:0}$. Although the $[M+H]^+$ ions of lactosylceramides at $C_{25:0}$ and $Ch_{24:1}$ had the same value at *m/z* 989 and could not be identified by infusion analysis, they were completely separated on the column. Their retention times were 17.3 min for $Ch_{24:1}$ and 24.6 min for $C_{25:0}$. The former had 2-hydroxylated fatty acyl chains and was more hydrophilic than the latter.

Lactosylceramides with the same carbon number of fatty acyl chain of saturated ($C_{24:0}$) at *m/z* 975, unsaturated ($C_{24:1}$) at *m/z* 973, and 2-hydroxylated ($Ch_{24:0}$) at *m/z* 991 fatty acyl chain moiety appeared at 22.2, 18.6, and 20.8 min on the chromatogram, respectively (Figs. 4B–D). These results suggest that lactosylceramides classified as unsaturated, 2-hydroxylated, and saturated fatty acyl chain were eluted in that order on the column.

### *Determination of molecular species of porcine-blood cell-derived lactosylceramides*

We also identified more than 33 different structures as molecular species from porcine-blood-cell-derived lactosylceramides (Fig. 5A). The profile was constructed

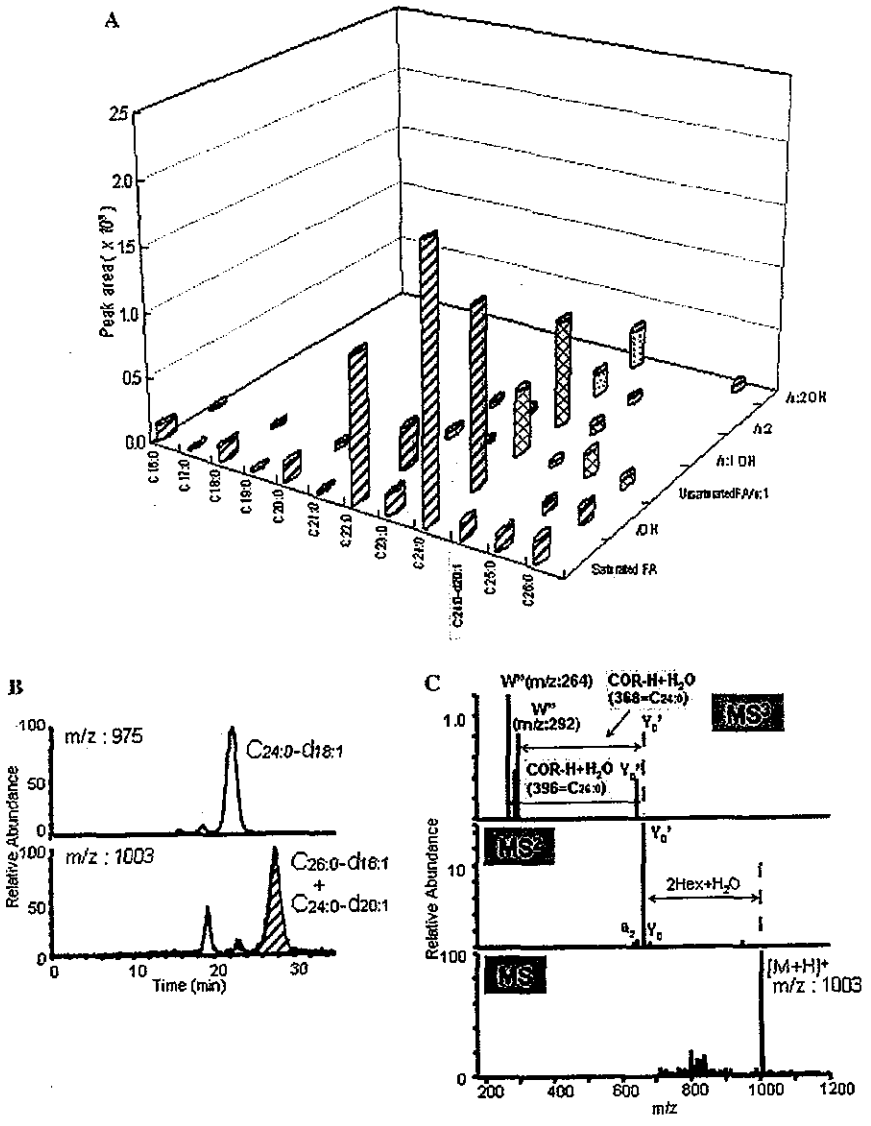


Fig. 5. Distribution of molecular species of lactosylceramides derived from porcine blood cells. (A) Abscissa represents the carbon unit of fatty acyl chain and long-chain base ($d_{18:1}$ is not shown). The intensity of lactosylceramides was estimated by the peak area on Figs. 3B–E. The ordinate represents the peak area. The *z* axis represents the class of fatty acyl chain such as saturated, unsaturated, and hydroxylated species. (B) The SIM chromatogram of the same $[M+H]^+$ ions at *m/z* 1003 for $C_{26:0}$-$d_{18:1}$ and $C_{24:0}$-$d_{20:1}$ and (C) $MS^n$ analysis ($n = 1$–3) for *m/z* 1003.

based on the peak area of SIM chromatogram for lactosylceramides. Some lactosylceramides with long-chain base moiety at $d_{20:1}$ were confirmed by $MS^3$ analysis and are shown in Fig. 5C. The retention time of lactosylceramide at *m/z* 1003 for $C_{26:0}$-$d_{18:1}$ or $C_{24:0}$-$d_{20:1}$ was 28 min in Fig. 5B, but the *m/z* 264 and *m/z* 292 ions were produced on the $MS^3$ spectrum. This means that there were two other types of w″ ions associated with $d_{18:1}$ and $d_{20:1}$ sphingenines. Therefore, it was considered that separation of lactosylceramides was based on total carbon chain length and numbers of double bonds in the fatty acyl chain and long-chain base. Thus, lactosylceramides at $C_n$-$d_x$ and $C_{n-2}$-$d_{x+2}$ were not separated on the column in the system, however, we could at least confirm by $MS^3$ analysis the presence or absence of the two types of lactosylceramides.

The molecular species of porcine-blood-cell-derived lactosylceramides contained more than 33 different structures, which were mainly $C_{24:0}$-$d_{18:1}$, $Ch_{24:0}$-$d_{18:1}$, $Ch_{24:1}$-$d_{18:1}$, $C_{24:1}$-$d_{18:1}$, and $C_{22:0}$-$d_{18:1}$, with 28 other minor species. Minor species of long-carbon-chain fatty acids such as $C_{22}$ and $C_{26}$ were also identified as saturated, unsaturated, and hydroxylated species. The number of molecular species of lactosylceramides determined by LC-ESI/MS was twice that confirmed by infusion analysis. The amount of lactosylceramides used was 200 ng for determination of the $[M + H]^+$ ions and automatic $MS^n$ analysis with LC-ESI/MS. In the case of infusion analysis, lactosylceramides at 10 ng/μl were infused into the ion source for 10–15 min depending on the number of $MS^n$ analyses of $[M + H]^+$ ions manually. The sample amounts used for both analyses were not different and LC-ESI/MS was convenient and precise for determination of low-intensity $[M + H]^+$ ions.

Since the standard compound of the molecular species of lactosylceramides could not be reported and no product could be identified, we were unable to perform quantification analysis of these species. However, the SIM chromatograms of 10–200 ng of porcine-blood-cell-derived lactosylceramides showed almost linear relationships between the ratio of the peak area and the total amount of lactosylceramides (data not shown).

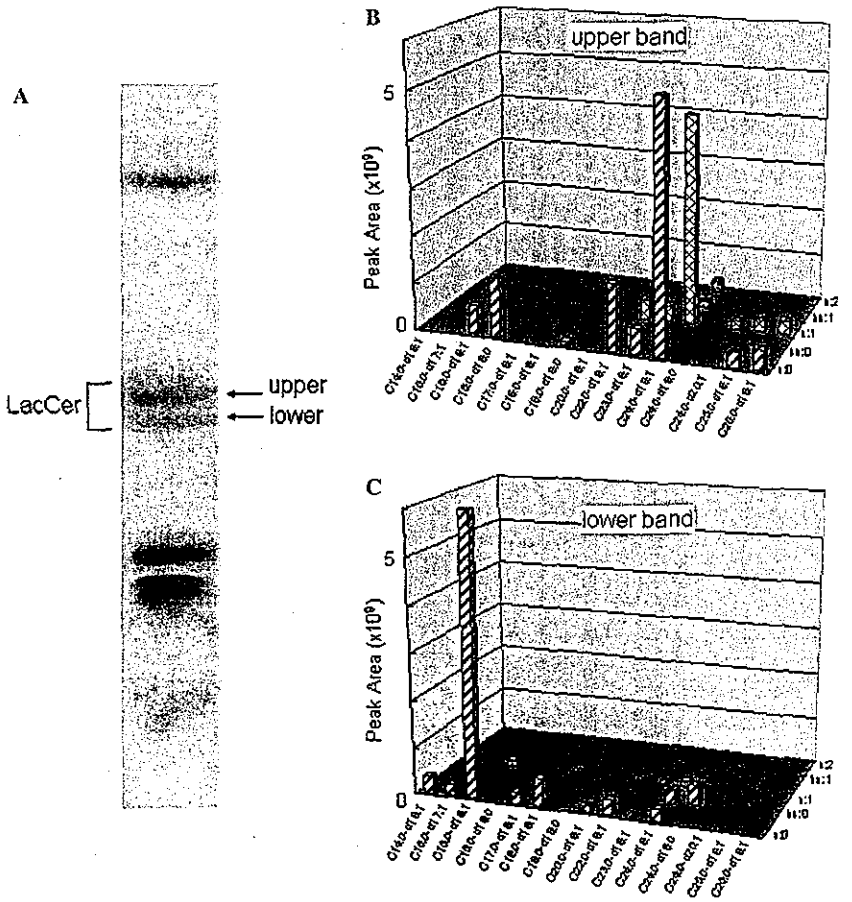


Fig. 6. Determination of molecular species of lactosylceramides derived from membrane microdomain of HL-60 cells. (A) The pattern of lactosylceramides for membrane microdomain fractionated from HL-60 cells separated on HPTLC. (B) Molecular species of lactosylceramides in the upper band and (C) those in the lower band derived from HL-60 cells ($8 \times 10^6$ cells). The abscissa, ordinate, and *z* axis are similar to those used in Fig. 5.

*Analysis of molecular species of lactosylceramides in the membrane microdomain fraction of HL-60 cells*

Crude lipids were extracted from the membrane microdomain fraction of HL-60 cells using a mixture of chloroform and methanol (2:1 v/v). A fifth of the crude lipids was separated on HPTLC with a mixture solution of chloroform/methanol/water (65:25:4 v/v/v) and detected by primulin reagent. Lactosylceramides marked as upper and lower bands in Fig. 6A were removed and collected in each glass tube and crude lactosylceramides were extracted with a mixture of chloroform and methanol (2:1 v/v). A fifth of the crude lactosylceramides was loaded on a column and determined by LC-ESI-$MS^n$ analysis, respectively. Figs. 6B and C show the distribution of molecular species of lactosylceramides in the upper and the lower bands, respectively. A total of 25 species of lactosylceramides was detected in the upper and lower bands on the HPTLC plate.

Lactosylceramides in the upper band consisted mainly of $C_{24:0}$-$d_{18:1}$, $C_{24:1}$-$d_{18:1}$, and $C_{22:0}$-$d_{18:1}$ and those in the lower band were mainly $C_{16:0}$-$d_{18:1}$ but higher carbon chain structures such as $Ch_{24:0}$-$d_{18:1}$ fatty acyl chain moiety at *m/z* 991 were also detected. The high molecular species in the lower band seemed to be insufficiently separated on the HPTLC plate and rather coexisted with those of the upper band. It is possible, however, that the hydrophilic property of $Ch_{24:0}$ could have affected the separation of lactosylceramides on the HPTLC plate. On the other hand, lactosylceramide for $C_{16:0}$-$d_{18:0}$ also appeared in the upper band, suggesting that it might be more hydrophobic than lactosylceramide for $C_{16:0}$-$d_{18:1}$ on the HPTLC plate. Numerous minor lactosylceramides that contained odd numbers of fatty acyl chains and saturated long-chain base moieties were identified also, although we could not clarify whether these structures have any biological relevance in HL-60 cells, of which about 70% differentiate into macrophage-lineage cells.

Further studies are necessary to identify key ions of various types of lactosylceramides such as branched, polyunsaturated fatty acyl moieties, and other types of sphingoids like phytosphingosine to characterize their structures and biological significance. There is also a need to determine the position of double bonds and hydroxylation in both fatty acyl chain and long-chain base moieties of lactosylceramides by LC-ESI ion trap mass spectrometry.

## Conclusions

Using mass spectrometry, lactosylceramide was ionized with alkaline metals or ammonium salts to produce molecular ions of $[M + Li/Na]^+$ at 400 °C or $[M + H]^+$ at 200 °C. The $[M + Li]^+$ ion was stable and not fragmented into fatty acyl chain and long-chain base moiety. However, $MS^3$ analysis showed some dissociation of lactosylceramide $[M + H]^+$ ion. The loss of two hexoses and water resulted in cleavage of the amide bond, which allowed information on the long chain base and fatty acyl moiety necessary to determine the molecular species of lactosylceramide to be obtained.

In the present study, we developed a useful and simple method to identify the molecular species of lactosylceramides using reverse-phase LC-ESI ion trap mass spectrometry. Using sequential $MS^n$ analysis, we could obtain in multiple steps the dissociation patterns of a single ion. The patterns became simple and allowed us to speculate on the structure of the molecular species. The obtained molecular species were classified as $[M + H]^+$ ions, which were produced with ammonium formate. In our analysis, 200 ng of lactosylceramides derived from porcine blood cells contained more than 33 molecular species. Lactosylceramides were eluted from a column depending on the length of their carbon chain and appeared in the order of unsaturated, 2-hydroxylated, and saturated fatty acyl chain with the same number of carbon atoms.

We also used our method to determine the molecular species of lactosylceramides present in the membrane microdomain fraction of HL-60 cells (about 70% were differentiated cells). Five species of major lactosylceramides and about 20 species of minor ones were detected in the upper and lower bands on the HPTLC plate. The biological relevance of the minor lactosylceramides, which consisted of about 20 species from $C_{16}$ to $C_{26}$, is not clear yet.

## Acknowledgments

We thank Professor Sandro Sonnino and Dr. Alessandro Prinetti from the Department of Medical Chemistry, Biochemistry and Biotechnology, University of Milan, Italy for their generous gift of some synthetic lactosylceramides used in this study. This work was supported in part by Grants-in-aid from the Ministry of Education, Culture, Sports, Science, and Technology of Japan 16017293 for K.I. This work was supported, in part, by Thermo Electron Corp.

## References

[1] K. Simons, D. Toomre, Lipid rafts and signal transduction, Nat. Rev. Mol. Cell Biol. 1 (2000) 31–39.
[2] S. Hakomori, Cell adhesion/recognition and signal transduction through glycosphingolipid microdomain, *Glycoconj.* J. 17 (2000) 143–151.
[3] K. Iwabuchi, I. Nagaoka, Lactosylceramide-enriched glycosphingolipid signaling domain mediates superoxide generation from human neutrophils, Blood 100 (2002) 1454–1464.

[4] T.Y. Wang, J.R. Silvius, Sphingolipid partitioning into ordered domains in cholesterol-free and cholesterol-containing lipid bilayers, Biophys. J. 84 (2003) 367–378.
[5] D. Hoekstra, O. Maier, J.M. Vander Wouden, T.A. Slimane, S.C.D. Van Ijzendoorn, Membrane dynamics and cell polarity: the role of sphingolipids, J. Lipid Res. 44 (2003) 869–877.
[6] X.M. Li, M.M. Momsen, H.L. Brockman, R.E. Brown, Lactosylceramide: effect of acyl chain structure on phase behavior and molecular packing, Biophys. J. 83 (2002) 1535–1546.
[7] C.E. Costello, J.E. Vath, Tandem mass spectrometry of glycolipids, Methods Enzymol. 193 (1990) 738–768.
[8] Q. Ann, J. Adams, Structure determination of ceramides and neutral glycosphingolipids by collisional activation of $[M + Li]^+$ ions, J. Am. Soc. Mass Spectrom. 3 (1992) 260–263.
[9] Q. Ann, J. Adams, Structure-specific collision-induced fragmentations of ceramides cationized with alkali-metal ions, Anal. Chem. 65 (1993) 7–13.
[10] R.S. Duarte, C.R. Polycarpo, R. Wait, R. Hartmann, E.B. Bergter, Structural characterization of neutral glycosphingolipids from *Fusarium* species, Biochim. Biophys. Acta 1390 (1998) 186–196.
[11] F.F. Hsu, J. Turk, Structural determination of glycosphingolipids as lithiated adducts by electrospray ionization mass spectrometry using low-energy collisional-activated dissociation on a triple stage quadrupole instrument, J. Am. Soc. Mass Spectrom. 12 (2001) 61–79.
[12] F.F. Hsu, J. Turk, Characterization of ceramides by low energy collisional-activated dissociation tandem mass spectrometry with negative-ion electrospray ionization, J. Am. Soc. Mass Spectrom. 13 (2002) 558–570.
[13] X. Han, Characterization and direct quantitation of ceramide molecular species from lipid extracts of biological samples by electrospray ionization tandem mass spectrometry, Anal. Biochem. 302 (2002) 199–212.
[14] G. Pocsfalvi, A. Malorni, I. Mancini, G. Guella, F. Pietra, Molecular characterization of a highly heterogeneous mixture of glucosylceramides from a deep-water Mediterranean scleractinian coral *Dendrophyllia cornigera*, Rapid Commun. Mass Spectrom. 14 (2000) 2247–2259.
[15] M.H. Lee, G.H. Lee, J.S. Yoo, Analysis of ceramides in cosmetics by reversed-phase liquid chromatography/electrospray ionization mass spectrometry with collision-induced dissociation, Rapid Commun. Mass Spectrom. 17 (2003) 64–75.
[16] B.J. Pettus, A. Bielawska, B.J. Kroesen, P.D.R. Moeller, Z.M. Szulc, Y.A. Hannun, M. Busman, Observation of different ceramide species from crude cellular extracts by normal-phase high-performance liquid chromatography coupled to atmospheric pressure chemical ionization mass spectrometry, Rapid Commun. Mass Spectrom. 17 (2003) 1203–1211.
[17] F. Sako, S. Gasa, A. Makita, A. Hayashi, S. Nozawa, Human blood group glycosphinglipids of porcine erythrocytes, Arch. Biochem. Biophys. 278 (1990) 228–237.

# Identification of Neurite Outgrowth Active Sites on the Laminin α4 Chain G Domain†

Naoki Ichikawa,[‡,§,∥] Shingo Kasai,[∥] Nobuharu Suzuki,[∥] Norio Nishi,[∥] Shinya Oishi,[⊥] Nobutaka Fujii,[⊥] Yuichi Kadoya,[@] Kozo Hatori,[§] Yoshikuni Mizuno,[§] Motoyoshi Nomizu,[∥] and Eri Arikawa-Hirasawa*[,‡,§]

*Research Institute for Diseases of Old Age and Department of Neurology, Juntendo University School of Medicine, Tokyo 113-8421, Japan, Graduate School of Environmental Earth Science, Hokkaido University, Sapporo 060-0810, Japan, Graduate School of Pharmaceutical Sciences, Kyoto University, Kyoto 606-8501, Japan, and Department of Anatomy, Kitasato University School of Medicine, Sagamihara 228-8555, Japan*

*Received November 9, 2004; Revised Manuscript Received January 16, 2005*

ABSTRACT: The laminin α4 chain is widely distributed in various mesodermal tissues, including the perineurium of peripheral nerves, dorsal root ganglion (DRG), skeletal muscle, and capillaries, and plays important roles in synaptic specialization at the neuromuscular junction and in microvascular formation. The C-terminal globular domain (G domain) of the laminin α4 chain was previously found to be critical for heparin binding and cell attachment activity. Here, we focused on neurite outgrowth activity of the laminin α4 chain G domain. We found that the recombinant α4 chain G domain protein (rec-α4G) promoted neurite outgrowth of rat pheochromocytoma PC12 cells. When 114 overlapping synthetic peptides that covered the entire G domain were tested for neurite outgrowth activity, nine peptides were active, but the 105 remaining peptides did not exhibit activity. Three of the nine active peptides, A4G6 (LAIKNDNLVYVY), A4G20 (DVISLYNFKHIY), and A4G107 (VIRDSNVVQLDV), strongly promoted neurite outgrowth of PC12 cells. A4G107 was found to form amyloid-like fibrils in Congo red, X-ray, and electron microscopy analyses. We also synthesized cyclic peptides to evaluate their conformational requirements. Cyclic peptide A4G82X (cyc-A4G82X;TLFLAHGRLVFX, where X is norleucine) significantly enhanced neurite outgrowth activity, but the rest of the cyclic peptides eliminated the activity. The A4G82 sequence is located on the loop region, suggesting that the activity of A4G82 is required for a loop conformation. These peptides also exhibited neurite outgrowth activity with dorsal root ganglion (DRG) explants and with DRG cells from E14.5 mouse embryos, indicating that they are active in both neuronal cell lines and native neuronal cells. Taken together, the data suggest that the peptides from the laminin α4 chain G domain promote neurite outgrowth activity via a specific conformation.

Laminins are a family of heterotrimeric extracellular matrix glycoproteins and are a major component of basement membranes. Laminins consist of α, β, and γ chains, and at least 15 isoforms have been identified with various combinations of five α, three β, and three γ chains (*1*–*4*). The laminin isoforms appear to have tissue-specific distributions and have various biological functions, including cell adhesion, neurite outgrowth, tumor metastasis, and angiogenesis (*1*, *4*). The functions of individual chains and isoforms have been elucidated from studies on genetic diseases and by targeted gene disruption in mice (*5*–*11*).

Laminins promote neurite outgrowth of peripheral and central nervous system neurons and many neuronal cell lines (*12*). Laminins have potential as a directional cue for migrating axons (*13*, *14*) and an important guidance molecule for developing axons (*15*). Several peptides derived from laminins have been found to promote neurite outgrowth (*16*–*19*). Large globular domains (G domain), consisting of LG1–LG5 modules, at the carboxyl terminus of laminin α chains have been suggested to play an important role in cellular interactions and biological activities (*20*). Several active peptides from the G domains of laminin α1 and α2 chains have been shown to stimulate neurite outgrowth (*21*). We also reported that the LG4 and LG5 modules of the laminin α3 chain G domain exhibited neurite outgrowth activity (*22*).

The laminin α4 chain is a component of three laminins: laminin 8 (α4:β1:γ1), laminin 9 (α4:β2:γ1), and the recently identified laminin 14 (α4:β2:γ3) (*1*, *23*). The α4 chain lacks the N-terminal short arm and is expressed in cells of a mesenchymal origin, such as endothelial cells and adipocytes (*24*, *25*). The laminin α4 chain is widely distributed in various mesodermal tissues, as well as the perineurium of peripheral nerves, dorsal root ganglion (DRG), heart, kidney, skeletal muscle, capillaries, and endothelium (*26*–*28*). Previous work using laminin α4-deficient mice has indicated that

† Part of this work was supported by Grants-in-Aid from the Ministry of Health, Labor and Welfare and Grant from the Ministry of Education, Culture, Sports, Science and Technology of Japan.

* To whom correspondence should be addressed: Research Institute for Diseases of Old Age, Juntendo University School of Medicine, Building 10, Room 606, 2-1-1 Hongo, Bunkyo-ku, Tokyo 113-8421, Japan. Telephone and fax: 81-3-3814-3016. E-mail: ehirasaw@med.juntendo.ac.jp.

‡ Research Institute for Diseases of Old Age, Juntendo University School of Medicine.

§ Department of Neurology, Juntendo University School of Medicine.

∥ Hokkaido University.

⊥ Kyoto University.

@ Kitasato University School of Medicine.

10.1021/bi0476228 CCC: $30.25 
Published on Web 00/00/0000 PAGE EST: 7.2

the laminin α4 chain has a significant role in newly formed capillary basement membranes and transsynaptically coordinates pre- and postsynaptic differentiation (*29*, *30*). In the absence of laminin α4, the active zone and transmitter release site at the growth cone and the junctional fold at the muscle site are formed but are not precisely apposed to each other (*30*), suggesting that laminin α4 at the growth cone regulates neuronal outgrowth and neuromuscular junction formation. Moreover, loss of laminin α2 leads to upregulation of laminin α4 throughout muscle basal laminae (*28*, *31*). It was demonstrated that the laminin α4 G domain was proteolytically processed in cultured endothelial and schwannoma cells, and the LG4−LG5 module of the α4 G domain was released (*32*). The α4 G domain binds to heparin, sulfatides, and fibulins (*32*). Using the recombinant protein and a large set of overlapping peptides, active sequences of the laminin α4 G domain for cell attachment and syndecan-2 or -4 binding were identified (*33*−*35*).

In this paper, we describe a systematic screening of neurite outgrowth active sequences in the mouse laminin α4 G domain (residues 852−1816) using a recombinant protein and 114 overlapping synthetic peptides covering the G domain. We identified several peptides active for promoting neurite outgrowth of rat phenochromocytoma PC12 cells and mouse E14.5 embryo DRG explants and cells. We also evaluated their conformational requirement for activity.

## MATERIALS AND METHODS

*Recombinant Protein (rec-α4G) and Synthetic Peptides.* A recombinant protein (rec-α4G) involving the mouse laminin α4 chain G domain (residues 852−1816) with a c-myc sequence at the C-terminus was expressed using *dhfr*-deficient CHO DG44 cells and purified with a heparin affinity column (HiTrap, Amersham Pharmacia Biotech, Uppsala, Sweden) and a gel filtration column (Superdex 200, Amersham Pharmacia Biotech), as previously described (*33*, *34*). The purity and amount of rec-α4G protein were monitored by 8% SDS−PAGE under reducing conditions. Pure fractions were combined, and the protein concentration was determined with the BCA assay (Pierce, Rockford, IL).

All peptides were synthesized manually using the 9-fluorenylmethoxycarbonyl (Fmoc)-based solid phase strategy and prepared in the C-terminal amide form as previously described (*34*, *36*). The purity and identity of the synthetic peptides were confirmed by reverse phase high-performance liquid chromatography (HPLC) and by fast atom bombardment mass spectral analysis at the GC-MS & NMR Laboratory, Graduate School of Agriculture, Hokkaido University. Two peptides (A4G98 and A4G99) were not soluble in aqueous solution and could not be purified by reverse phase HPLC. The A4G82 sequence contains a methionine residue at the C-terminus. To prevent oxidization during synthesis, the methionine residue was replaced with norleucine (A4G82X). Cyclic peptides were synthesized by adding cysteine to the carboxyl- and amino-terminal ends of each peptide (Table 2) and cyclizing under oxidative conditions (45:10:45 $CH_3COOH$/DMSO/$H_2O$ mixture), a modified method described previously (*37*).

*Culture of Cells.* PC12 cells (*38*) were cultured in Dulbecco's modified Eagle's medium (DMEM, Gibco, Grand Island, NY) containing 7.5% horse serum (Gibco), 7.5% fetal bovine serum (FBS, Gibco), 100 units/mL penicillin, and 100 μg/mL streptomycin (Gibco).

Table 1: Neurite Outgrowth Activity of Peptides on the Laminin α4 Chain G Domain[a]

| peptide | sequence | neurite outgrowth[b] |
|---|---|---|
| A4G6 | $^{892}$LAIKNDNLVYVY$^{903}$ | +++ |
| A4G20 | $^{1009}$DVISLYNFKHIY$^{1020}$ | ++ |
| A4G51 | $^{1261}$LOPNGLLFYYTSG$^{1273}$ | + |
| A4G82X | $^{1514}$TLFLAHGRLVFX$^{1525\,c}$ | + |
| A4G93 | $^{1598}$NVQITSVYSFSG$^{1609}$ | + |
| A4G94 | $^{1611}$LGNLOLNGASIT$^{1622}$ | + |
| A4G95 | $^{1619}$ASITSASOTFSVT$^{1631}$ | + |
| A4G107 | $^{1729}$VIRDSNVVOLDV$^{1740}$ | +++ |
| A4G116 | $^{1800}$KAALVSGAVSINS$^{1812}$ | + |
| AG73[d] | RKRLQVQLSIRT | +++ |

[a] The sequences and residues of the peptides were derived from the mouse laminin α4 chain (GenBank accession number AAC24725). [b] Neurite outgrowth-promoting activities of the peptides with PC12 cells were evaluated by the following subjective scale: +++, activity comparable to that on AG73; ++, activity apparent but weaker than that on AG73; +, activity significantly low. [c] The C-terminal residue of A4G82 is methionine (residue 1525). Because the methionine residue is easily oxidized during the synthesis, we replaced it with norleucine (X). This replacement did not change the HT1080 cell attachment activity (*34*). [d] AG73 was used as a positive control for neurite outgrowth activity (*21*, *42*).

Table 2: Sequences of Cyclic Peptides and Neurite Outgrowth Activity

| peptide | sequence | neurite outgrowth[a] |
|---|---|---|
| A4G6 | LAIKNDNLVYVY | +++ |
| cyc-A4G6 | CLAIKNDNLVYVYC | − |
| A4G20 | DVISLYNFKHIY | ++ |
| cyc-A4G20 | CDVISLYNFKHIYC | − |
| A4G82X | TLFLAHGRLVFX[b] | + |
| cyc-A4G82X | CTLFLAHGRLVFX[b]C | +++ |
| A4G107 | VIRDSNVVOLDV | +++ |
| cyc-A4G107 | CVIRDSNVVOLDVC | − |
| AG73[c] | RKRLOVOLSIRT | +++ |

[a] Neurite outgrowth-promoting activities of the peptides with PC12 cells were evaluated by the following subjective scale: +++, activity comparable to that on AG73; ++, activity apparent but weaker than that on AG73; +, activity significantly low; −, no activity. [b] C-Terminal methionine residue A4G82 was replaced with norleucine (X). [c] AG73 was used as a positive control for neurite outgrowth activity (*21*, *42*).

*Neurite Outgrowth Assay Using a Recombinant Protein and Synthetic Peptides.* The neurite outgrowth assay using proteins and peptides was performed in 96- and 24-well plates (Nunc), as previously described (*22*). The recombinant protein in 50 μL of 10 mM Tris-HCl (pH 7.4), 150 mM NaCl, 2 mM EDTA, and 0.5 mM *N*-ethylmaleimide (buffer A) and laminin in 50 μL of Milli-Q water were added to 96-well plates and the plates incubated overnight at 4 °C. Synthetic peptides dissolved in 500 μL of Milli-Q water were added to 24-well plates and the plates dried overnight. Plates coated with proteins or peptides were washed with DMEM/F12 (Gibco). PC12 cells were primed with 100 ng/mL nerve growth factor (NGF, Roche Applied Science, Indianapolis, IN) for 24 h prior to the assay. The PC12 cells were then collected by agitation, allowed to recover in the cultured medium for 30 min at 37 °C in 5% $CO_2$, and then washed three times with DMEM/F12. After being washed, cells were resuspended in DMEM/F12 containing 100 μg/mL transferrin (Sigma), 20 nM progesterone (Sigma), 30 nM $Na_2SeO_3$

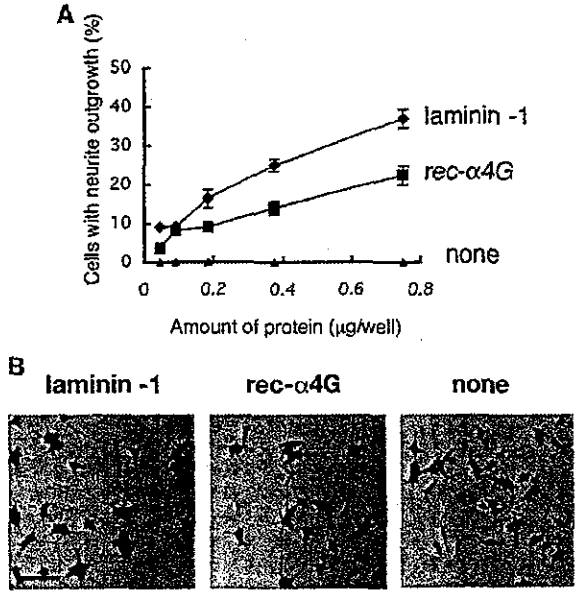


FIGURE 1: Neurite outgrowth activity of the recombinant rec-α4G protein in PC12 cells. (A) Various amounts of rec-α4G and laminin 1 were coated on 96-well plates, and PC12 cells ($2 \times 10^4$ cells/well) were seeded in the plates. After being incubated for 24 h, cells were fixed and stained. The percentage of neurite outgrowth cells was determined as described in Materials and Methods. Data are expressed as mean ± SD of triplicate results. (B) The PC12 cells cultured on rec-α4G (1.2 μg/well) and laminin 1 (1.2 μg/well) for 24 h were stained with crystal violet and photographed on a microscope (200×). The scale bar is 100 μm.

(Wako, Osaka, Japan), 5 μg/mL insulin (Gibco), and 100 ng/mL NGF. The cells were added to 96- and 24-well plates at densities of $3.0 \times 10^3$ and $2.0 \times 10^4$ cells/well, respectively. The cells were incubated at 37 °C for 24 h and fixed with 20% formalin, and then the number of cells equal to or greater than twice the cell diameter was determined and averaged for each peptide tested.

A neurite outgrowth assay of DRG cells and explants was performed as described previously (*39*, *40*), with some modifications. DRG cells and explants were obtained from mouse E14.5 embryos, and other non-neuronal tissues were removed carefully. DRGs were collected in ice-cold PBS and incubated with 0.25% trypsin and DNase for 30 min at 37 °C. DRG cells collected by centrifugation (1000 rpm for 8 min). The cells and explants were incubated in 0.5% N2 supplement, 50 ng/mL NGF, and 1% PSM DMEM/F12 for 24 h on poly-L-lysine (10 μg/mL), and A4G6, A4G20, A4G82X, cyclic-A4G82X, and A4G107 (50 μg/mL) coated coverglasses. Neurite length was measured by confocal laser microscopy (Carl Zeiss LSM510 instrument).

*Congo Red Binding Analysis.* Peptides (1.0 mg/mL) in phosphate-buffered saline (PBS) and Congo red solution (100 μM in PBS) were mixed and incubated in disposable cuvettes for 24 h at room temperature. Absorption spectra were measured from 300 to 700 nm using a U-2000A UV–vis spectrophotometer (Hitachi Co. Ltd., Tokyo, Japan).

*Congo Red Staining and Polarized Light Microscopy.* A4G6, A4G20, and A4G107 were dissolved in PBS at a concentration of 5 mg/mL. The solutions were pipetted onto glass slides and dried overnight. The precipitates were stained with a 1% aqueous solution of Congo red for 1 h. After being

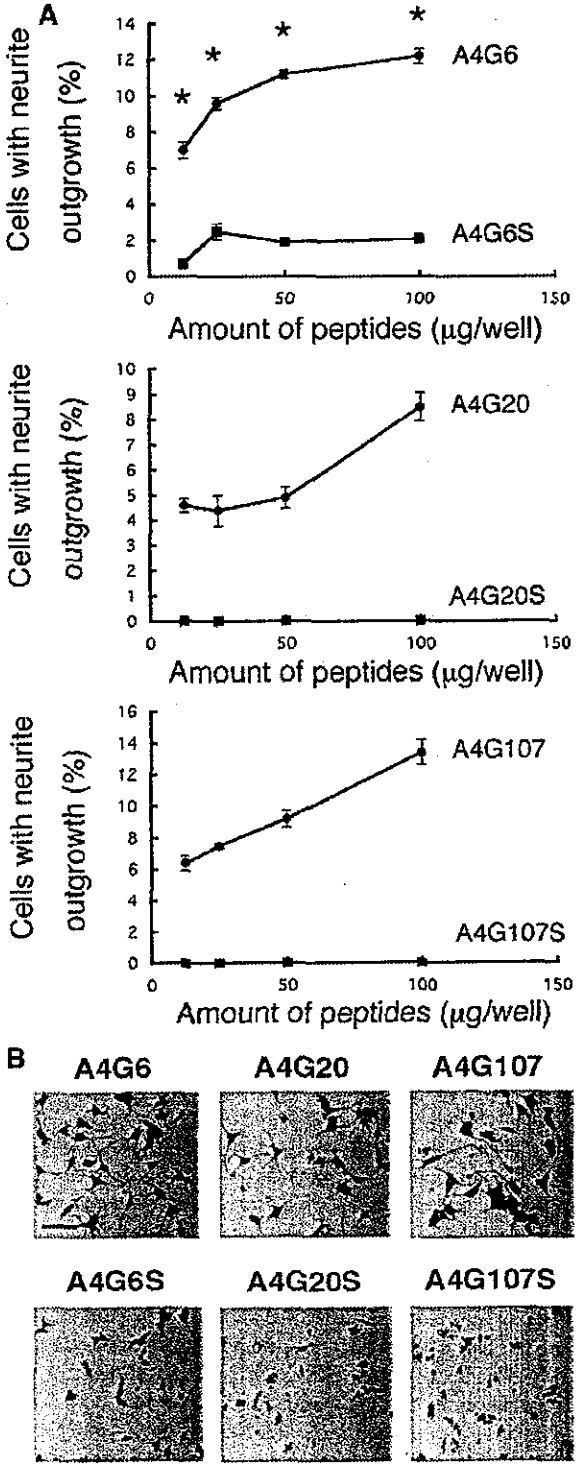


FIGURE 2: Neurite outgrowth of PC12 cells on synthetic peptides. (A) Various amounts of peptides were coated on 24-well plates. PC12 cells ($2 \times 10^4$ cells/well) were seeded in the plates. After being incubated for 24 h, cells were fixed and stained. The percentage of neurite outgrowth cells was determined as described in Materials and Methods. Triplicate experiments gave similar results (asterisk indicates $p < 0.01$). (B) The PC12 cells were cultured on various peptides (50 μg/well) for 24 h, stained with crystal violet, and then photographed on a microscope (200×). S represents the scrambled peptide. The scale bar is 100 μm.

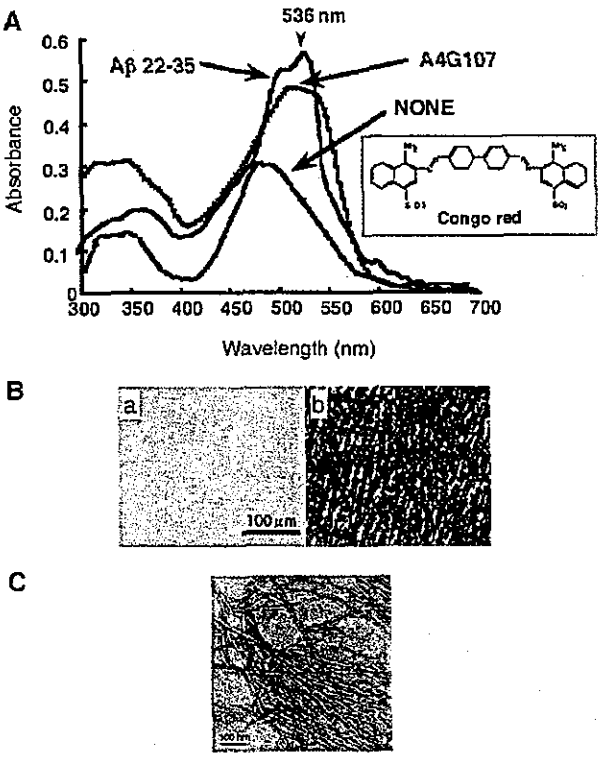


FIGURE 3: Congo red staining analysis and amyloid-like fibrils of A4G107. (A) A Congo red solution (100 $\mu$M) and a peptide solution (2 mg/mL) were mixed in PBS at room temperature for 24 h, and UV spectra were measured from 300 to 700 nm. (B) A4G107 in PBS (5 mg/mL) was pipetted onto a glass slide. After drying overnight, the precipitate was stained with a 1% aqueous solution of Congo red for 1 h. After being rinsed with pure acetone, samples were dehydrated as described in Materials and Methods. The specimens were mounted with a resin and observed in a microscope either under bright field illumination or between crossed polars. (C) Amyloid-like fibrils of A4G107. A4G107 (1 mg) was dissolved in PBS (200 $\mu$L), and the resulting gel was kept at 4 °C for 1 week. The amyloid-like fibrils were stained with a 5% aqueous solution of uranyl acetate and observed using an electron microscope.

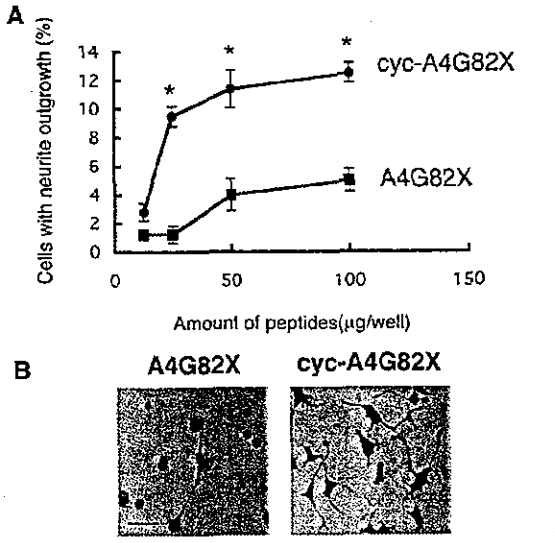


FIGURE 4: Neurite outgrowth activity of the cyclic peptide. (A) Various amounts of A4G82X and cyc-A4G82X peptides were coated on 24-well plates. PC12 cells ($2 \times 10^4$ cells/well) were seeded in the plates. After being incubated for 24 h, cells were fixed and stained. The percentage of neurite outgrowth cells was determined as described in Materials and Methods. Assays was repeated three times (asterisk indicates $p < 0.01$). (B) The PC12 cells were cultured on A4G82X and cyc-A4G82X peptide-coated plates (50 $\mu$g/well) for 24 h, stained with crystal violet, and then photographed on a microscope (200×). The scale bar is 100 $\mu$m.

rinsed with pure acetone, the samples were dehydrated with 95 and 100% ethanol and then cleared with xylene. The specimens were mounted with a resin (malinol, Muto Pure Chemicals, Tokyo, Japan) and observed in a microscope (AX80, Olympus, Tokyo, Japan) either under bright field illumination or between crossed polar.

*Electron Microscopy.* Peptide gel in Milli-Q water (5 mg/mL) was applied onto a carbon-coated grid mesh with a thin Formvar film. The specimen was then negatively stained with a 5% aqueous solution of uranyl acetate and observed using a JEM-1200EX (JEOL, Tokyo, Japan) electron microscope at an acceleration voltage of 80 kV.

*Immunocytochemistry.* DRG explants were cultured for 24 h on peptide- or poly-L-lysine-coated coverglasses, fixed by 4% parafolmaldehyde in PBS for 10 min at room temperature, and blocked with 5% donkey serum (Chemicon International, Inc., Temecula, CA) and 1% BSA in PBS for 15 min. The primary antibody, rabbit anti-neurofilament (Sigma), was added and left at 4 °C overnight. The cells were then incubated with Alexa 488-conjugated donkey anti-rabbit IgG (Molecular Probes, Engene, OR) for 1 h at room temperature. After washing had been carried out, immunostained images were analyzed on a confocal laser microscope (Carl Zeiss LSM510 instrument).

## RESULTS

*Neurite Outgrowth Activity of the Rec-α4G Protein.* A recombinant protein (rec-α4G) containing the mouse laminin α4 G domain and the c-myc sequence at the C-terminus was expressed in *dhfr*-deficient CHO DG44 cells and purified as previously described (*33*). Neurite outgrowth activity of the rec-α4G protein was tested using PC12 cells. Laminin 1 as a control promoted neurite outgrowth as described previously (*4*). The rec-α4G protein also promoted neurite outgrowth activity in a dose-dependent manner (Figure 1A,B). These results indicated that the laminin α4 G domain promotes neurite outgrowth and that active sequences exist in the domain.

*Neurite Outgrowth Activity of Synthetic Peptides.* We prepared 116 overlapping peptides covering the mouse laminin α4 G domain (*34*). One hundred fourteen peptides were soluble, but two peptides were not. The 114 soluble peptides were tested for their neurite outgrowth activity in PC12 cells. AG73 in the laminin α1 chain G domain was previously found to promote neurite outgrowth and was used as a control (*21*, *41*, *42*). Nine peptides promoted neurite outgrowth activity with PC12 cells (Table 1). A4G6, A4G20, and A4G107 showed especially strong neurite outgrowth activity in a dose-dependent manner, but scrambled peptides of these active peptide sequences were inactive (Figure 2A,B).

*Congo Red Staining Analysis.* The neurite outgrowth activity of IKVAV, derived from laminin α1, was recently reported to be closely related to amyloid-like fibril formation (*43*). Accordingly, the ability of the three active peptides to

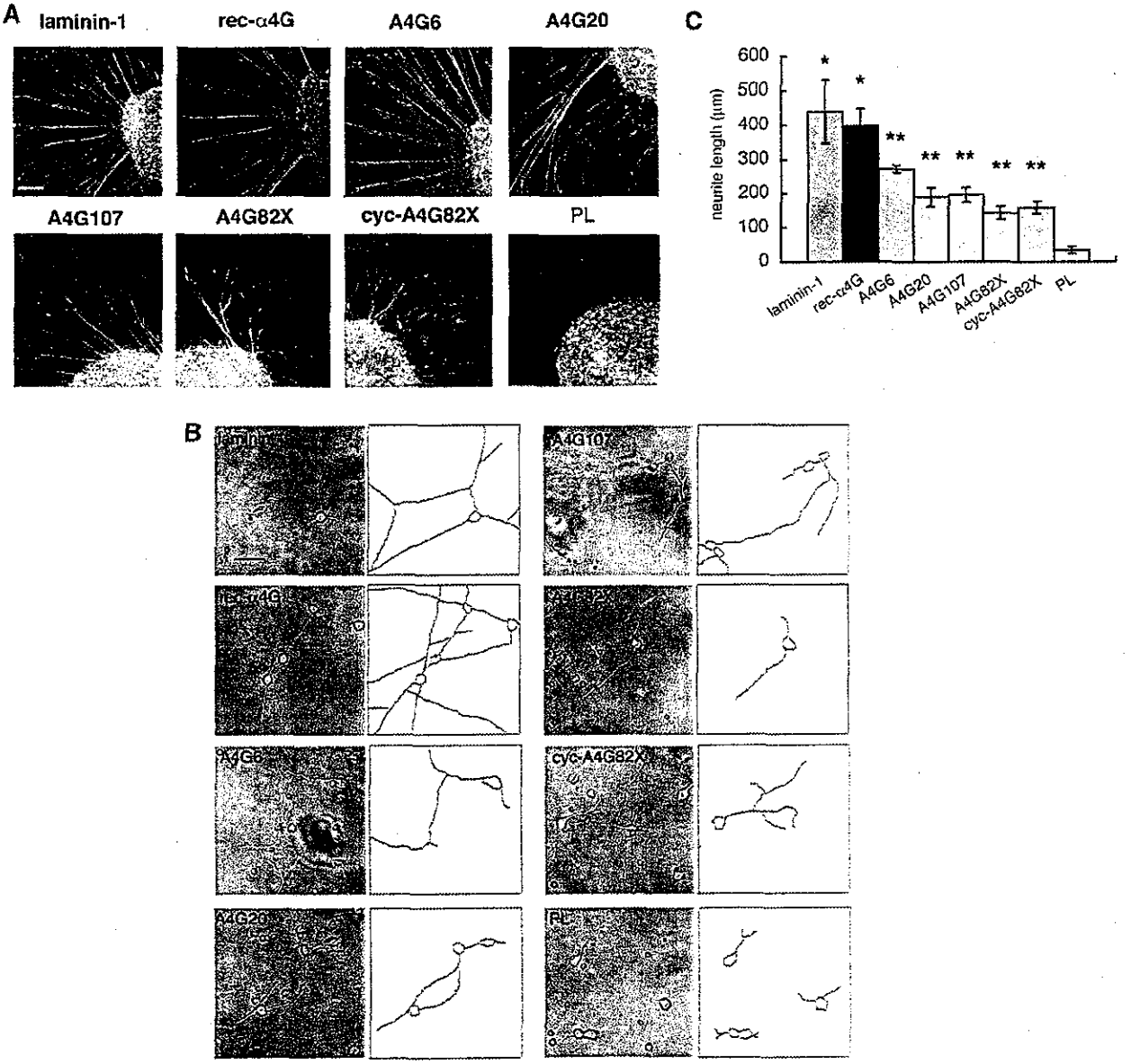


FIGURE 5: Neurite outgrowth of DRG explants (A) and cells (B) on peptide-, rec-α4G-, and laminin 1-coated coverglasses. DRG explants (A) and cells (B), prepared as described in Materials and Methods, were cultured for 24 h on poly-L-lysine (PL) (10 μg/mL)-, peptide (50 μg/well)-, rec-α4G (1.2 μg/mL)-, and laminin 1 (1.2 μg/mL)-coated coverglasses. (A) DRG explants were immunostained with the antibody against neurofilaments. (B) Primary cells from DRG were photographed on a confocal laser microscope (Carl Zeiss LSM510) and traced using NIH Image. (C) The neurite length of primary DRG cells ($n = 30$) was measured and analyzed using NIH Image (one asterisk indicates $p < 0.0001$; two asterisks indicate $p < 0.001$). The scale bar is (A) 50 or (B) 100 μm.

form amyloid-like fibrils was tested using Congo red (*44*). The absorption spectrum of the Congo red solution showed a peak at 486 nm as described previously (*43*, *45*). Two large peaks (at 512 and 536 nm) only appeared after the Congo red solution was incubated with A4G107 for 24 h (Figure 3A) but not when incubated with other peptides. These wavelengths were specific for the complex of Congo red and amyloid-like fibrils such as amyloid β-peptides (*45*). When the A4G107/Congo red solution was dried and examined under a polarizing microscope, the peptide precipitate exhibited birefringence, changing from red to green (Figure 3B). Negative staining electron microscopy showed that the A4G107 peptide formed a gel with the appearance of amyloid-like fibrils (Figure 3C). The scrambled peptide of A4G107 did not form amyloid-like fibrils (data not shown). These results suggest that the A4G107 peptide forms an amyloid-like structure and specifically binds to Congo red.

*Neurite Outgrowth Activity of the Cyclic Peptide.* We previously reported that the peptides, located in the loop region of the laminin α4 chain G domain, had biological activity (*22*, *34*). A4G82X, which is located in the loop region of the laminin α4 G domain, weakly promoted neurite outgrowth activity (Table 1). A4G82X and three other active peptides, A4G6, A4G20, and A4G107, were synthesized cyclically, and those peptides were tested for neurite outgrowth activity with PC12 cells (Table 2). The cyc-A4G82X peptide enhanced the activity (Figure 4), but the remaining cyclic peptides completely lost their activity (Table

2). These results suggest that the neurite outgrowth activity of the peptides depends on the conformation.

*Neurite Outgrowth Activity of the Rec-α4G Protein and Synthetic Peptides on DRG Explants and Cells.* The effects of rec-α4G and synthetic peptides (A4G6, A4G20, A4G82X, cyc-A4G82X, and A4G107) on mouse E14.5 embryo dorsal root ganglion (DRG) explants and cells were examined next. The rec-α4G protein showed a strong activity for neurite outgrowth of both DRG explants (Figure 5A) and cells (Figure 5B,C). The A4G6, A4G20, A4G82X, cyc-A4G82X, and A4G107 peptides also promoted neurite outgrowth of the DRG cells and explants, but poly-L-lysine did not exhibit activity at 24 h (Figure 5). Therefore, these peptides are active for promoting neurite outgrowth of native neuronal cells.

## DISCUSSION

The laminin α4 chain is expressed in the perineurium of the peripheral nerves and a part of the brain and is implicated in the regulation of neuronal network formation (*1*, *23*, *26*, *32*). In this report, we showed that the recombinant laminin α4 G domain promoted neurite outgrowth, and we identified active sites for the activity within the domain by screening 114 synthetic peptides overlapping almost the entire laminin α4 G domain. We found that nine of the 114 peptides were active for neurite outgrowth of PC12 cells, and three of these peptides, A4G6, A4G20, and A4G107, exhibited stronger activity. We previously demonstrated that these three peptides were also strongly active for HT1080 cell attachment and heparin binding (*34*). A4G82X exhibiteded strong activity for HT1080 cell attachment and heparin binding (*34*), but we found that it was relatively weak for neurite outgrowth-promoting activity with PC12 cells. However, we found that cyclization of A4G82X significantly increased the activity, while all other cyclic peptides lost their neurite outgrowth-promoting activity, suggesting conformation-dependent activity.

Among the active peptides, A4G107 was found to form amyloid-like fibrils but A4G6 and A4G20 were not, suggesting that the amyloid-like structure is not a prerequisite for the neurite outgrowth-promoting activity of some peptides. However, the amyloid-like structure of A4G107 is likely necessary for neurite promoting activity, since the scrambled peptide of A4G107 lost amyloid formation and neurite outgrowth-promoting activity. As for A4G107, we recently reported that the IKVAV-containing peptide from the laminin α1 chain formed amyloid-like fibrils and was active for promoting neurite outgrowth and cell adhesion (*43*). We showed that these biological activities of the IKVAV-containing peptide were associated with amyloid-like fibril formation (*43*). Insoluble amyloid-like fibrils formed by assembly of β sheet domains are involved in several pathological conditions, including Alzheimer's and Huntington diseases (*46*, *47*). Laminin and its fragments interact with amyloid proteins and may be associated with amyloid formation (*48*, *49*). The IKVAV-containing peptide was shown to bind to the 110 kDa amyloid precursor protein (*48*). The A4G107 site of the laminin α4 chain may also interact with amyloid precursor proteins and be involved in amyloid plaque formation.

The G domain of laminin α chains has been implicated in many biological activities (*20*). Although it has a similar domain structure in all laminin α chains, its biological activities appear to be chain-specific (*20*). The laminin α4 chain G domain is proteolytically processed in vivo and in cultured endothelial and Schwannoma cells, resulting in the release of the LG4−LG5 part from the α4 chain (*32*). Both proteolytic fragments were able to bind heparin and cells (*32*, *35*); however, the biological significance of the processing is not clear. The LG4 subdomains of the laminin α chains consist of a 14-stranded β-sheet (A to N) sandwich structure, and several active sites in the connective region within the subdomain were identified. Recently, 19-mer peptides (EF peptides) were prepared from the E and F strands of the LG4 domains from five laminin α chains and compared for their activities (*37*). These studies showed that each EF peptide has unique cell type- and chain-specific biological activities. Peptide EF-4 from the laminin α4 chain, which contains the A4G82 sequence, attached to fibroblasts and promoted neurite outgrowth of PC12 cells (*37*). Using a crystal structure-based sequential alignment study of laminin α2 and α4 chains, A4G82 was shown to be located in the loop region between β strands in the LG4 module (*20*, *35*). The cyclic A4G82X peptide mimics the loop structure in this region. Therefore, neurite outgrowth-promoting activity of A4G82X is likely required for a loop conformation. Previously, we reported that the A3G75 peptide from the laminin α3 LG4 domain located on the loop region promotes cell adhesion and neurite outgrowth (*22*, *37*). A cyclic A3G75 may have stronger activity on neurite outgrowth than A3G75, similar to A4G82.

Recently, A4G6, A4G20, and cyclic A4G82X were found to interact with either syndecan-2 or -4 (*34*, *50*). Syndecans have been shown to work cooperatively with integrins (*51*) for cellular signaling, and the laminin α4 G domain binds both integrins and syndecans. It is possible that the neurite outgrowth-promoting activity of the peptides is regulated by both syndecans and integrins. This may explain why the peptides are less active for neurite outgrowth, compared to the recombinant rec-α4G protein, containing the whole G domain of the laminin α4 chain.

## ACKNOWLEDGMENT

We thank Drs. M. Hoffman and Y. Yamada for valuable comments on the manuscript.

## REFERENCES

1. Miner, J. H., Patton, B. L., Lentz, S. I., Gilbert, D. J., Snider, W. D., Jenkins, N. A., Copeland, N. G., and Sanes, J. R. (1997) The laminin α chains: Expression, developmental transitions, and chromosomal locations of α1−5, identification of heterotrimeric laminins 8−11, and cloning of a novel α3 isoform, *J. Cell Biol. 137*, 685−701.
2. Iivanainen, A., Morita, T., and Tryggvason, K. (1999) Molecular cloning and tissue-specific expression of a novel murine laminin γ3 chain, *J. Biol. Chem. 274*, 14107−14111.
3. Libby, R. T., Champliaud, M. F., Claudepierre, T., Xu, Y., Gibbons, E. P., Koch, M., Burgeson, R. E., Hunter, D. D., and Brunken, W. J. (2000) Laminin expression in adult and developing retinae: Evidence of two novel CNS laminins, *J. Neurosci. 20*, 6517−6528.
4. Colognato, H., and Yurchenco, P. D. (2000) Form and function: The laminin family of heterotrimers, *Dev. Dyn. 218*, 213−234.
5. Pulkkinen, L., Christiano, A. M., Airenne, T., Haakana, H., Tryggvason, K., and Uitto, J. (1994) Mutations in the γ2 chain gene (LAMC2) of kalinin/laminin 5 in the junctional forms of epidermolysis bullosa, *Nat. Genet. 6*, 293−297.

6. Aberdam, D., Galliano, M. F., Vailly, J., Pulkkinen, L., Bonifas, J., Christiano, A. M., Tryggvason, K., Uitto, J., Epstein, E. H., Jr., Ortonne, J. P., et al. (1994) Herlitz's junctional epidermolysis bullosa is linked to mutations in the gene (LAMC2) for the γ2 subunit of nicein/kalinin (LAMININ-5), *Nat. Genet. 6*, 299−304.
7. McGrath, J. A., Kivirikko, S., Ciatti, S., Moss, C., Dunnill, G. S., Eady, R. A., Rodeck, C. H., Christiano, A. M., and Uitto, J. (1995) A homozygous nonsense mutation in the α3 chain gene of laminin 5 (LAMA3) in Herlitz junctional epidermolysis bullosa: Prenatal exclusion in a fetus at risk, *Genomics 29*, 282−284.
8. Helbling-Leclerc, A., Zhang, X., Topaloglu, H., Cruaud, C., Tesson, F., Weissenbach, J., Tome, F. M., Schwartz, K., Fardeau, M., Tryggvason, K., et al. (1995) Mutations in the laminin α2-chain gene (LAMA2) cause merosin-deficient congenital muscular dystrophy, *Nat. Genet. 11*, 216−218.
9. Tome, F. M., Evangelista, T., Leclerc, A., Sunada, Y., Manole, E., Estournet, B., Barois, A., Campbell, K. P., and Fardeau, M. (1994) Congenital muscular dystrophy with merosin deficiency, *C. R. Acad. Sci. III 317*, 351−357.
10. Xu, H., Wu, X. R., Wewer, U. M., and Engvall, E. (1994) Murine muscular dystrophy caused by a mutation in the laminin α2 (Lama2) gene, *Nat. Genet. 8*, 297−302.
11. Miner, J. H., Cunningham, J., and Sanes, J. R. (1998) Roles for laminin in embryogenesis: Exencephaly, syndactyly, and placentopathy in mice lacking the laminin α5 chain, *J. Cell Biol. 143*, 1713−1723.
12. Powell, S. K., and Kleinman, H. K. (1997) Neuronal laminins and their cellular receptors, *Int. J. Biochem. Cell Biol. 29*, 401−414.
13. Kuhn, T. B., Schmidt, M. F., and Kater, S. B. (1995) Laminin and fibronectin guideposts signal sustained but opposite effects to passing growth cones, *Neuron 14*, 275−285.
14. Kuhn, T. B., Williams, C. V., Dou, P., and Kater, S. B. (1998) Laminin directs growth cone navigation via two temporally and functionally distinct calcium signals, *J. Neurosci. 18*, 184−194.
15. Forrester, W. C., and Garriga, G. (1997) Genes necessary for *C. elegans* cell and growth cone migrations, *Development 124*, 1831−1843.
16. Tashiro, K., Sephel, G. C., Weeks, B., Sasaki, M., Martin, G. R., Kleinman, H. K., and Yamada, Y. (1989) A synthetic peptide containing the IKVAV sequence from the A chain of laminin mediates cell attachment, migration, and neurite outgrowth, *J. Biol. Chem. 264*, 16174−16182.
17. Hunter, D. D., Porter, B. E., Bulock, J. W., Adams, S. P., Merlie, J. P., and Sanes, J. R. (1989) Primary sequence of a motor neuron-selective adhesive site in the synaptic basal lamina protein S-laminin, *Cell 59*, 905−913.
18. Hunter, D. D., Cashman, N., Morris-Valero, R., Bulock, J. W., Adams, S. P., and Sanes, J. R. (1991) An LRE (leucine-arginine-glutamate)-dependent mechanism for adhesion of neurons to S-laminin, *J. Neurosci. 11*, 3960−3971.
19. Liesi, P., Narvanen, A., Soos, J., Sariola, H., and Snounou, G. (1989) Identification of a neurite outgrowth-promoting domain of laminin using synthetic peptides, *FEBS Lett. 244*, 141−148.
20. Timpl, R., Tisi, D., Talts, J. F., Andac, Z., Sasaki, T., and Hohenester, E. (2000) Structure and function of laminin LG modules, *Matrix Biol. 19*, 309−317.
21. Richard, B. L., Nomizu, M., Yamada, Y., and Kleinman, H. K. (1996) Identification of synthetic peptides derived from laminin α1 and α2 chains with cell type specificity for neurite outgrowth, *Exp. Cell Res. 228*, 98−105.
22. Kato, K., Utani, A., Suzuki, N., Mochizuki, M., Yamada, M., Nishi, N., Matsuura, H., Shinkai, H., and Nomizu, M. (2002) Identification of neurite outgrowth promoting sites on the laminin α3 chain G domain, *Biochemistry 41*, 10747−10753.
23. Frieser, M., Nockel, H., Pausch, F., Roder, C., Hahn, A., Deutzmann, R., and Sorokin, L. M. (1997) Cloning of the mouse laminin α4 cDNA. Expression in a subset of endothelium, *Eur. J. Biochem. 246*, 727−735.
24. Tokida, Y., Aratani, Y., Morita, A., and Kitagawa, Y. (1990) Production of two variant laminin forms by endothelial cells and shift of their relative levels by angiostatic steroids, *J. Biol. Chem. 265*, 18123−18129.
25. Sorokin, L. M., Pausch, F., Frieser, M., Kroger, S., Ohage, E., and Deutzmann, R. (1997) Developmental regulation of the laminin α5 chain suggests a role in epithelial and endothelial cell maturation, *Dev. Biol. 189*, 285−300.
26. Iivanainen, A., Kortesmaa, J., Sahlberg, C., Morita, T., Bergmann, U., Thesleff, I., and Tryggvason, K. (1997) Primary structure, developmental expression, and immunolocalization of the murine laminin α4 chain, *J. Biol. Chem. 272*, 27862−27868.
27. Lefebvre, O., Sorokin, L., Kedinger, M., and Simon-Assmann, P. (1999) Developmental expression and cellular origin of the laminin α2, α4, and α5 chains in the intestine, *Dev. Biol. 210*, 135−150.
28. Patton, B. L., Miner, J. H., Chiu, A. Y., and Sanes, J. R. (1997) Distribution and function of laminins in the neuromuscular system of developing, adult, and mutant mice, *J. Cell Biol. 139*, 1507−1521.
29. Thyboll, J., Kortesmaa, J., Cao, R., Soininen, R., Wang, L., Iivanainen, A., Sorokin, L., Risling, M., Cao, Y., and Tryggvason, K. (2002) Deletion of the laminin α4 chain leads to impaired microvessel maturation, *Mol. Cell. Biol. 22*, 1194−1202.
30. Patton, B. L., Cunningham, J. M., Thyboll, J., Kortesmaa, J., Westerblad, H., Edstrom, L., Tryggvason, K., and Sanes, J. R. (2001) Properly formed but improperly localized synaptic specializations in the absence of laminin α4, *Nat. Neurosci. 4*, 597−604.
31. Ringelmann, B., Roder, C., Hallmann, R., Maley, M., Davies, M., Grounds, M., and Sorokin, L. (1999) Expression of laminin α1, α2, α4, and α5 chains, fibronectin, and tenascin-C in skeletal muscle of dystrophic 129ReJ dy/dy mice, *Exp. Cell Res. 246*, 165−182.
32. Talts, J. F., Sasaki, T., Miosge, N., Gohring, W., Mann, K., Mayne, R., and Timpl, R. (2000) Structural and functional analysis of the recombinant G domain of the laminin α4 chain and its proteolytic processing in tissues, *J. Biol. Chem. 275*, 35192−35199.
33. Yamaguchi, H., Yamashita, H., Mori, H., Okazaki, I., Nomizu, M., Beck, K., and Kitagawa, Y. (2000) High and low affinity heparin-binding sites in the G domain of the mouse laminin α4 chain, *J. Biol. Chem. 275*, 29458−29465.
34. Okazaki, I., Suzuki, N., Nishi, N., Utani, A., Matsuura, H., Shinkai, H., Yamashita, H., Kitagawa, Y., and Nomizu, M. (2002) Identification of biologically active sequences in the laminin α4 chain G domain, *J. Biol. Chem. 277*, 37070−37078.
35. Yamashita, H., Beck, K., and Kitagawa, Y. (2004) Heparin binds to the laminin α4 chain LG4 domain at a site different from that found for other laminins, *J. Mol. Biol. 335*, 1145−1149.
36. Nomizu, M., Kuratomi, Y., Malinda, K. M., Song, S. Y., Miyoshi, K., Otaka, A., Powell, S. K., Hoffman, M. P., Kleinman, H. K., and Yamada, Y. (1998) Cell binding sequences in mouse laminin α1 chain, *J. Biol. Chem. 273*, 32491−32499.
37. Suzuki, N., Nakatsuka, H., Mochizuki, M., Nishi, N., Kadoya, Y., Utani, A., Oishi, S., Fujii, N., Kleinman, H. K., and Nomizu, M. (2003) Biological activities of homologous loop regions in the laminin α chain G domains, *J. Biol. Chem. 278*, 45697−45705.
38. Greene, L. A., and Tischler, A. S. (1976) Establishment of a noradrenergic clonal line of rat adrenal pheochromocytoma cells which respond to nerve growth factor, *Proc. Natl. Acad. Sci. U.S.A. 73*, 2424−2428.
39. Hayashita-Kinoh, H., Kinoh, H., Okada, A., Komori, K., Itoh, Y., Chiba, T., Kajita, M., Yana, I., and Seiki, M. (2001) Membrane-type 5 matrix metalloproteinase is expressed in differentiated neurons and regulates axonal growth, *Cell Growth Differ. 12*, 573−580.
40. Ivins, J. K., Yurchenco, P. D., and Lander, A. D. (2000) Regulation of neurite outgrowth by integrin activation, *J. Neurosci. 20*, 6551−6560.
41. Nomizu, M., Kim, W. H., Yamamura, K., Utani, A., Song, S. Y., Otaka, A., Roller, P. P., Kleinman, H. K., and Yamada, Y. (1995) Identification of cell binding sites in the laminin α1 chain carboxyl-terminal globular domain by systematic screening of synthetic peptides, *J. Biol. Chem. 270*, 20583−20590.
42. Weeks, B. S., Nomizu, M., Ramchandran, R. S., Yamada, Y., and Kleinman, H. K. (1998) Laminin-1 and the RKRLQVQLSIRT laminin-1 α1 globular domain peptide stimulate matrix metalloproteinase secretion by PC12 cells, *Exp. Cell Res. 243*, 375−382.
43. Yamada, M., Kadoya, Y., Kasai, S., Kato, K., Mochizuki, M., Nishi, N., Watanabe, N., Kleinman, H. K., Yamada, Y., and Nomizu, M. (2002) Ile-Lys-Val-Ala-Val (IKVAV)-containing laminin α1 chain peptides form amyloid-like fibrils, *FEBS Lett. 530*, 48−52.
44. Klunk, W. E., Pettegrew, J. W., and Abraham, D. J. (1989) Quantitative evaluation of congo red binding to amyloid-like proteins with a β-pleated sheet conformation, *J. Histochem. Cytochem. 37*, 1273−1281.